Journal of Sound and Vibration 332 (2013) 3750-3767

Surface modes in sheared boundary layers over impedance linings*

E.J. Brambley†

DAMTP, University of Cambridge, Wilberforce Road, Cambridge CB3 0WA, UK

Received 27 October 2012; received in revised form 13 February 2013; accepted 22 February 2013

Abstract

Surface modes, being duct modes localized close to the duct wall, are analysed within a lined cylindrical duct with uniform flow apart from a thin boundary layer. As well as full numerical solutions of the Pridmore-Brown equation, simplified mathematical models are given where the duct lining and boundary layer are lumped together and modelled using a single boundary condition (a modification of the Myers boundary condition previously proposed by the author), from which a surface mode dispersion relation is derived. For a given frequency, up to six surface modes are shown to exist, rather than the maximum of four for uniform slipping flow. Not only is the different number and behaviour of surface modes important for frequency-domain mode-matching techniques, which depend on having found all relevant modes during matching, but the thin boundary layer is also shown to lead to different convective and absolute stability than for uniform slipping flow. Numerical examples are given comparing the predictions of the surface mode dispersion relation to full solutions of the Pridmore-Brown equation, and the accuracy with which surface modes are predicted is shown to be significantly increased compared with the uniform slipping flow assumption. The importance of not only the boundary layer thickness but also its profile (tanh or linear) is demonstrated. A Briggs–Bers stability analysis is also performed under the assumption of a mass–spring–damper or Helmholtz resonator impedance model.

Keywords: Surface mode, boundary layer, impedance lining, stability.

1 Introduction

As a simplified mathematical model for the propagation of sound in an aeroengine intake or bypass, consider an acoustically-lined cylindrical or annular duct with an axial mean flow. The acoustic lining is represented by a impedance $Z(\omega) = p/v$, where an oscillatory pressure $p\exp\{\mathrm{i}\omega t\}$ produces an oscillating normal fluid velocity $v\exp\{\mathrm{i}\omega t\}$ at the lining. The simplest mean axial flow is a uniform flow (a flow constant across the duct), which would at first seem to be a good approximation for aeroengines owing to the high Reynolds numbers at which they operate. This situation has been extensively studied using the Myers [2], or Ingard–Myers [3], boundary condition, which incorporates both the impedance of the boundary and the effect of slipping mean flow. This boundary condition has been shown by Eversman & Beckemeyer [4] and Tester [5] to correspond to the limit of a vanishingly-thin inviscid non-slip boundary layer over the impedance boundary.

We note two important features of a uniform flow over an impedance boundary using the Myers boundary condition. The first is that, in addition to the acoustic modes (expected to be only slightly perturbed from their hard-wall counterparts due to the boundary impedance), modes of a different nature localized close to the boundary are also supported. These modes were investigated initially by Rienstra [6], who aptly named them *surface modes*, and subsequently by Brambley & Peake [7]. For a locally-reacting boundary, meaning that Z is a

*A preliminary version of this work [1] was presented as AIAA paper 2011–2736 at the 17th AIAA/CEAS Aeroacoustics Conference, 6–8 June 2011, Portland, Oregon, USA.

†Corresponding author. Tel.: +44 1223 760457. Fax.: +44 1223 765900.. Email: E.J.Brambley@damtp.cam.ac.uk

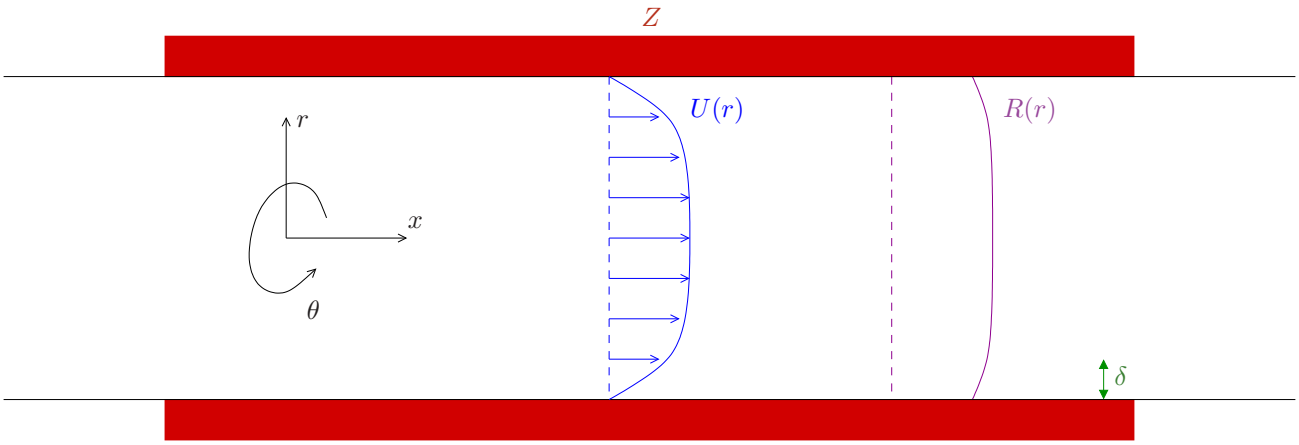

Figure 1: Sketch of the geometry considered here: a cylindrical lined duct in the x-direction containing mean axial flow of velocity $U(r)$ and density $R(r)$, uniform except within a thin boundary layer of width $O(\delta)$. The mean flow temperature $T_0(r) \propto 1/R(r)$.

function only of the frequency ω and is independent of wavelength, at any frequency there are up to four surface modes, one of which was tentatively suggested by Rienstra [6] as being a hydrodynamic instability. The second important feature of this uniform flow over an impedance boundary using the Myers boundary condition is that it yields an illposed problem [8], meaning that numerical simulations become unstable at the grid scale, that a rigorous stability analysis is not possible, and that frequency-domain simulations are of ambiguous accuracy.

Recently, progress has been made on correcting this illposedness by incorporating a thin-but-nonzero thickness boundary layer over the impedance boundary, leading to so called *modified Myers boundary conditions* by Rienstra & Darau [9, 10], Joubert [11], and Brambley [12, 13], some of which are compared by Gabard [14]. These boundary conditions aim to remove the illposedness while still retaining the simplicity of a uniform flow, with the thin-but-nonzero-thickness boundary layer being incorporated within the boundary condition. These modified Myers boundary conditions lead to a modified impedance Z_{mod} which is in general a function of both frequency ω and axial wavenumber k even when the underlying impedance of the boundary is locally-reacting and is therefore independent of k. This extra dependence is expected to cause an increase in the number of surface modes above the four previously predicted; a similar effect has been seen for a thin cylindrical shell whose impedance includes a k^4 term, leading to up to ten surface modes for any given frequency [15]. It should be noted that these modified Myers boundary conditions are restricted to having thin inviscid boundary layers, and also ignore the possible presence of a critical layer within the boundary layer. Indications are that critical layers may be neglected provided there are no sound sources within the boundary layer [16], while the effect on the duct modes of viscosity within the boundary layer is small at the high frequencies of interest in aeroacoustics [13, 17]. However, Renou & Aurégan [18, 19] showed that in some circumstances accounting for viscosity within the boundary layer is necessary for accuracy reproducing experimental results, while here we will occasionally see hints of the presence of a critical layer.

The number and behaviour of the surface modes is of the utmost importance for verifying that a mode-matching scheme is considering all appropriate modes, and for stability analysis. For stability analyses this is particularly pertinent, since an absolute instability is given using the Briggs–Bers criterion [20, 21] by the collision of two modes in the k-plane as $\text{Im}(\omega)$ is varied, and hence if there are more surface modes there is more potential for an absolute instability to be present. Therefore, after first deriving in §2 the surface mode approximation that will be used throughout, we analyse the possible number of surface modes and their locations in §3. The accuracy of the surface mode approximation is verified by comparison with less approximate analytical and exact numerical solutions in §4, following which we consider the stability of the surface modes, including any possible absolute instabilities, in §5.

2 Mathematical derivation

While what follows is applicable to a cylindrical, annular, or planar impedance boundary, for definiteness here we will consider the cylindrical case only. The geometry we consider is shown in figure 1. The cylinder axis is in the x-direction with the cross-section defined by polar coordinates r, θ, and the cylinder contains a compressible fluid of density $R(r)$ flowing with a mean velocity $U(r)\boldsymbol{e_x}$ at a pressure p_0. Since p_0 is necessarily constant,

the mean flow temperature $T_0(r) \propto 1/R(r)$, so that one can think of specifying a mean flow temperature distribution $1/R(r)$ instead of specifying a mean flow density distribution $R(r)$. Nondimensionalizing by the duct radius, the centreline mean-flow sound speed and the centreline mean-flow density gives $R(0) = 1$ and the mean-flow centreline velocity as the Mach number $M = U(0)$. On top of this mean flow we consider small perturbations governed by the linearized Euler equations. Eliminating all variables but the pressure perturbation gives solutions of the form $p = p_0 + p_m(r;\omega,k)\exp\{\mathrm{i}\omega t - \mathrm{i}kx - \mathrm{i}m\theta\}$, where p_m satisfies the cylindrical Pridmore-Brown equation [22]

$$p_m'' + \left(\frac{1}{r} + \frac{2kU'}{\omega - Uk} - \frac{R'}{R}\right)p_m' + \left((\omega - Uk)^2 R - k^2 - \frac{m^2}{r^2}\right)p_m = 0, \tag{1}$$

where a prime denotes $\mathrm{d}/\mathrm{d}r$. For a uniform flow, where $R(r) \equiv 1$ and $U(r) \equiv M$, equation (1) simplifies to Bessel's equation, so that

$$p_m(r;\omega,k) = \mathrm{J}_m(\alpha r) \qquad \text{with} \qquad \alpha^2 = (\omega - Mk)^2 - k^2, \tag{2}$$

where J_m is the m^{th} Bessel function of the first kind. In this case, the boundary condition at the impedance boundary at $r = 1$ is given by the Myers boundary condition,

$$1 - \frac{(\omega - Mk)^2}{\mathrm{i}\omega Z_{\text{mod}}}\frac{\mathrm{J}_m(\alpha)}{\alpha \mathrm{J}_m'(\alpha)} = 0, \tag{3}$$

with $Z_{\text{mod}} = Z$, which is the dispersion relation giving, for example, the allowable axial wavenumbers k given ω and m.

In this paper we consider non-slipping axial flows with $U(r)$ and $R(r)$ constant outside a thin boundary layer of width of order $\delta \ll 1$, as depicted in figure 1. We model this using a modified Myers boundary condition incorporating the boundary layer into the boundary condition at $r = 1$, which therefore retains the simplicity of solutions in terms of Bessel functions given by (2). Here, the modified Myers boundary condition of Brambley [Eq. 9 of 13] is used, chosen in light of its good agreement [14] with full numerical simulations of the Pridmore-Brown equation (1). This boundary condition is also of the form of (3), but with

$$\mathrm{i}\omega Z_{\text{mod}} = \mathrm{i}\omega Z\left[1 - \left(k^2 + m^2\right)\delta I_1 \frac{\mathrm{J}_m(\alpha)}{\alpha \mathrm{J}_m'(\alpha)}\right] + \omega^2\delta_0 - 2\omega k M \delta_1 + k^2 M^2 \delta_k + O\left(\delta^2\right), \tag{4a}$$

where

$$\delta_0 = \int_0^1 1 - R(r)\,\mathrm{d}r, \qquad \delta_1 = \int_0^1 1 - \frac{R(r)U(r)}{M}\,\mathrm{d}r, \qquad \delta_k = \int_0^1 1 - \frac{R(r)U(r)^2}{M^2}\,\mathrm{d}r, \tag{4b}$$

$$\delta I_1 = \int_0^1 1 - \frac{(\omega - Mk)^2}{\left(\omega - U(r)k\right)^2 R(r)}\,\mathrm{d}r \sim \frac{\delta_s M k}{\omega} \quad \text{for} \quad k/\omega \gg 1, \qquad \text{where} \quad \delta_s = \frac{-M}{R(1)U'(1)}. \tag{4c}$$

Note that all δ quantities are of the order of the boundary layer thickness and so are small: δ_1 is the displacement thickness of the boundary layer; the momentum thickness is $\delta_2 = \delta_k - \delta_1$; and δ_s is also a measure of boundary layer thickness based on the mean flow surface shear stress. Here, we will use the asymptotic result of Ref. 13 for δI_1 given in (4c), while noting that this approximation of δI_1 is arguably in the relevant regime for surface modes (see §5.1 and [8]) and is exact for a linear boundary layer profile (such as was assumed by Rienstra & Darau [10] for their modified Myers boundary condition). The validity of this approximation may be inferred from the generally good match with numerical results that follow.

In this paper we are particularly interested in surface modes, for which the solution (2) and the dispersion relation (3,4) can be further simplified. The surface mode dispersion relation used here is that of Brambley & Peake [7], which is an extension of that given by Rienstra [6] to account for nonzero m. In slightly different notation to Ref. 7, the surface mode dispersion relation is

$$\mu - \frac{(\omega - Mk)^2}{\mathrm{i}\omega Z_{\text{mod}}} = 0 \qquad \text{where} \quad \mu^2 = k^2 + m^2 - (\omega - Mk)^2, \tag{5}$$

and $\mathrm{Re}(\mu)$ is required positive, since the eigenfunction for this surface mode is asymptotically $p_m(r)/p_m(1) \sim \exp\{-(1-r)\mu\}$ and is required to decay away from the surface. (Note that $\mathrm{i}\mu$ may be regarded as an approximate radial modal wave number.) Since $\mathrm{J}_m(\alpha)/\left(\alpha \mathrm{J}_m'(\alpha)\right) = p_m(1)/p_m'(1) \sim 1/\mu$, incorporating the modified Myers boundary condition (4) into (5) gives

$$\mu - \frac{(\omega - Mk)^2}{\mathrm{i}\omega Z\left(1 - \delta_s\left(k^2 + m^2\right)Mk/(\omega\mu)\right) + \omega^2\delta_0 - 2\omega k M \delta_1 + k^2 M^2 \delta_k} = 0, \tag{6}$$

which may be rearranged to give

$$\big(\mathrm{i}\omega Z+\omega^2\delta_0-2\omega kM\delta_1+k^2M^2\delta_k\big)^2\big(k^2+m^2-(\omega-Mk)^2\big)\omega^2 - \big(\mathrm{i}\omega Z\delta_s\big(k^2+m^2\big)Mk+\omega(\omega-Mk)^2\big)^2=0. \quad (7)$$

Assuming that Z is locally reacting, so that Z is independent of k and m, equation (7) gives a polynomial in k of degree six, so that there are six surface modes, although due to the restriction that $\mathrm{Re}(\mu)>0$ not all of these may be physical for all values of Z; a similar argument was used in Refs. 6 and 7. Indeed, the results of these two papers are recovered by setting the δ-quantities in (7) to zero, yielding a polynomial of degree four and therefore leading to four surface modes. If Z is given by a mass–spring–damper model, so that $\mathrm{i}\omega Z$ is a polynomial of degree two in ω, then for fixed k equation (7) gives a polynomial in ω of degree eight, so that there are eight possible surface modes in ω for fixed k. This compares to the unmodified Myers result of six surface modes, obtained by setting the δ-quantities in (7) to zero. Examples of the results of (7) are given in sections 3, 4 & 5.

The limitations of (7) should be borne in mind: that δI_1 is evaluated using the asymptotics given in (4c) which are only valid for $k/\omega\gg 1$; that the surface mode dispersion relation (5) is only valid for $\mathrm{Re}(\mu)\gtrsim O(1)$; that, since the surface modes have $\mathrm{J}_m(\alpha r)/\mathrm{J}_m(\alpha)\sim\exp\{-(1-r)\mu\}$, the modified Myers boundary condition (4) is only valid for surface modes provided $|\mu|\lesssim O(1/\delta)$, where δ is a typical boundary layer thickness; and that the modified Myers boundary condition (4) ignores the critical layer within the boundary layer. These last two limitations are the most serious, and to avoid them requires a different analysis, such as given by Brambley, Darau & Rienstra [16] for a constant-then-linear boundary layer profile of constant density.

2.1 The thin-boundary-layer limit

We have seen above that, for any given frequency ω, for a nonzero-thickness boundary layer there are up to six surface modes, while for a zero thickness boundary layer there are a maximum of four surface modes. It is therefore interesting to consider the behaviour of the surface modes in the limit of a thin boundary layer $\delta\to 0$, where δ_0/δ, δ_1/δ, δ_k/δ and δ_s/δ are held fixed. Writing the dispersion relation (7) as $a_0+a_1k+\cdots+a_6k^6$, by calculation it can be seen that $a_6=O(\delta^2)$ and $a_5=O(\delta)$, while all the other coefficients are $O(1)$. There are therefore two distinguished limits, being $k=O(1)$ and $k=O(1/\delta)$. As $\delta\to 0$, four of the surface modes tend to their zero-thickness boundary layer values and remain $O(1)$, while the other two surface modes follow the other distinguished limit and tend to infinity as

$$k=\frac{-\omega M}{\mathrm{i}\omega Z\delta_s\pm\omega\delta_k M\sqrt{1-M^2}}+O(1). \quad (8)$$

For $\mathrm{Re}(Z)>0$ and real ω these are both in the upper-half k-plane. Although either may have a corresponding $\mathrm{Re}(\mu)<0$ and therefore not be substantiated, it can be show that both are present for real ω and sufficiently small δ provided $|\omega\,\mathrm{Im}(Z)|>2$. Since, for large k to leading order, $\mu=\pm k\sqrt{1-M^2}+O(1)$, this in effect means that as $\delta\to 0$ and the boundary layer disappears, two of the surface modes disappear within it. This should be contrasted with, for example, the analysis of §5.1, which demonstrates important stability behaviour in a regime where the surface modes extend well beyond the boundary layer thickness.

2.2 Rescaling the surface mode dispersion relation

We may simplify the dispersion relation (7), reducing the number of free parameters by one, by introducing renormalized variables

$$\tilde\mu=\mu/m,\qquad \beta=+\sqrt{1-M^2},\qquad \sigma=M+\beta^2k/\omega,\qquad \lambda=\omega/(m\beta),$$
$$\tilde h=2\omega\delta_1,\qquad \Delta_0=\delta_0/(2\delta_1),\qquad \Delta_k=\delta_k/(2\delta_1),\qquad \Delta_s=\delta_s/(2\delta_1). \quad (9)$$

The *reduced axial wavenumber* σ was introduced by Rienstra [6] to remove the mean flow dependence from the axial wavenumber k, while $(\tilde\mu,\beta,\sigma,\lambda)$ are the same as $(\mu,\beta,\sigma,\lambda)$ of Brambley & Peake [7]. Using these, and assuming $m>0$, gives

$$\tilde\mu^2=1-\lambda^2\big(1-\sigma^2\big)\qquad\text{with}\quad \mathrm{Re}(\tilde\mu)>0, \quad (10)$$

while (6) gives the rescaled dispersion relation

$$\frac{\tilde\mu}{\beta\lambda}-\frac{(1-M\sigma)^2+\mathrm{i}Z\tilde h\Delta_sM(\sigma-M)\Big((\sigma-M)^2/\beta^2+1/\lambda^2\Big)}{\mathrm{i}Z\beta^4+\tilde h\big[\Delta_0\beta^4-M\beta^2(\sigma-M)+M^2\Delta_k(\sigma-M)^2\big]}=0. \quad (11)$$

The free parameters governing the behaviour of the surface modes are therefore the boundary impedance Z, the acoustic spinning parameter λ, the flow parameters M and $\tilde{h}$, and the boundary layer shape parameters Δ_0, Δ_k, and Δ_s. (Note that $\Delta_k = (1+1/H)/2$, where $H = \delta_1/\delta_2$ is the shape factor of the boundary layer.) A constant-then-linear boundary layer profile with constant density,

$$U(r) = \begin{cases} M & r < 1-h \\ M(1-r)/h & r > 1-h \end{cases} \qquad R(r) \equiv 1, \tag{12}$$

gives $\Delta_0 = 0$, $\Delta_k = 2/3$ and $\Delta_s = 1$, with $\tilde{h} = \omega h$.

In what follows, the rescaled variables (9) will be used for analysing the number and location of surface modes, as they remove the shift due to the mean flow and give results directly comparable with the previous results of Rienstra [6] and Brambley & Peake [7]. However, when analysing stability by taking $\mathrm{Im}(\omega) \neq 0$ we return to the unscaled variables, since then the dependence of ω on k becomes important.

2.3 Collision points

When solving the dispersion relation (7) for the allowable values of k (the surface modes), as the other parameters are varied the roots of the dispersion relation move, and it may happen that two surface modes collide for particular values of the parameters. For example, we might fix all parameters except for the impedance, and then ask what values of the impedance Z lead to a collision of surface modes, and where in the k-plane the collision take place. Equivalently, we may consider the rescaled dispersion relation (11) and ask for which values of Z there is a collision in the σ-plane. Rearranging (11) leads to

$$\mathrm{i}Z - \frac{(1-M\sigma)^2 - A\tilde{\mu}/\lambda\beta}{\beta^3\tilde{\mu}/\lambda - B} = 0, \tag{13a}$$

with

$$A = \tilde{h}\beta^4\Delta_0 - \tilde{h}M\beta^2(\sigma-M) + \tilde{h}M^2\Delta_k(\sigma-M)^2, \tag{13b}$$

$$B = \tilde{h}\Delta_s M(\sigma-M)\big((\sigma-M)^2/\beta^2 + 1/\lambda^2\big). \tag{13c}$$

Differentiating (13) with respect to σ and setting the result equal to zero gives, after rearranging and squaring to eliminate terms involving $\tilde{\mu}$ to an odd power,

$$\lambda^2\big[2M(1-M\sigma)\beta^4\tilde{\mu}^2 - AB\sigma\lambda^2 - 2M\tilde{\mu}^2BC + (1-M\sigma)^2\sigma\lambda^2\beta^4 + M\tilde{\mu}^2AD\big]^2 - M^2\beta^2\tilde{\mu}^2\big[2B(1-M\sigma)\lambda^2 - 2\tilde{\mu}^2C\beta^2 + D(1-M\sigma)^2\lambda^2\big]^2 = 0 \tag{14a}$$

where

$$C = M\tilde{h}\Delta_k(\sigma-M) - \tilde{h}\beta^2/2, \qquad D = \tilde{h}\Delta_s\big(3(\sigma-M)^2/\beta^2 + 1/\lambda^2\big), \tag{14b}$$

and $\tilde{\mu}^2$ is given by (10). Since (14) is a twelfth order polynomial in σ, there are therefore at most twelve such collision points, although some of these will correspond to $\mathrm{Re}(Z) < 0$ or $\mathrm{Re}(\tilde{\mu}) < 0$ and must therefore be discounted. Only the actual collision points satisfying both $\mathrm{Re}(Z) > 0$ and $\mathrm{Re}(\tilde{\mu}) > 0$ are plotted in the figures that follow (for example, figures 2 and 3). Note that these collision points are different to double roots, as described in §5, since the impedance Z will in general be a function of frequency ω.

3 The number and location of surface modes

In this section, we investigate the number and position of surface modes for a given frequency ω, and how these vary with varying impedance Z. The procedure we follow is similar to that proposed by Rienstra [6] and also followed by Brambley & Peake [7].

For a locally-reacting impedance, the surface mode dispersion relation (7) (or equivalently (11)) is of sixth order in k (or σ), and therefore there are six possible surface modes for a given frequency ω. However, not all of these potential surface modes will satisfy the requirement that $\mathrm{Re}(\mu) > 0$. The number of actual surface modes will therefore change when one of the potential surface modes moves from having $\mathrm{Re}(\mu) < 0$ to $\mathrm{Re}(\mu) > 0$. We may therefore map the curve $\mathrm{Re}(\mu) = 0$ into the complex Z-plane to determine regions of the Z-plane that have the same number of actual surface modes. Moreover, since only impedances that satisfy $\mathrm{Re}(Z) > 0$ remove

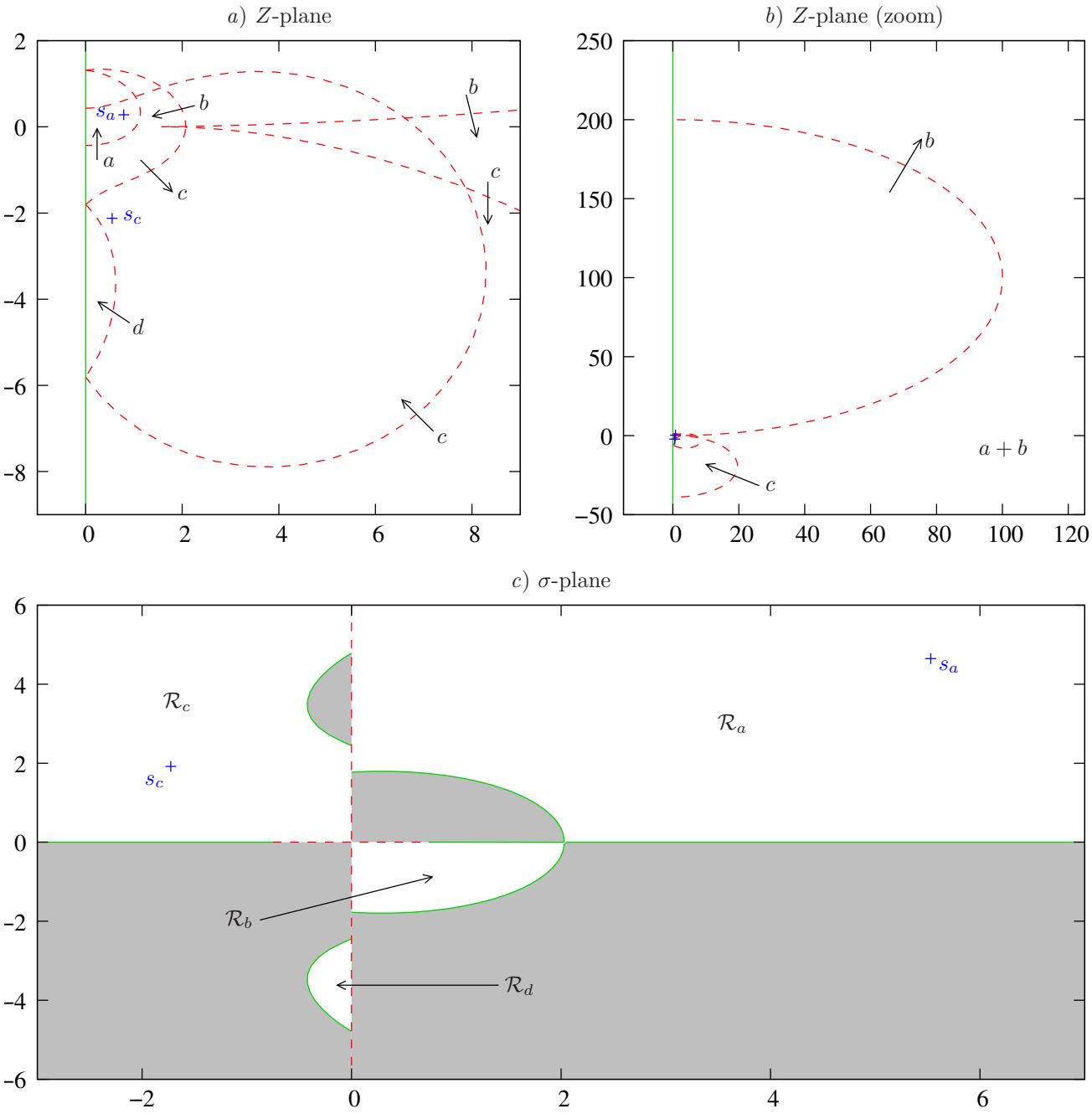

Figure 2: Plots of $\mathrm{Re}(\mu) = 0$ (dashed lines) and $\mathrm{Re}(Z) = 0$ (solid lines) in the Z- and σ-planes using the surface mode dispersion relation (7), for a tanh boundary layer profile given by (15) with $\delta = 10^{-3}$ and $M = 0.5$, for $\omega = 31$ and $m = 24$ (giving $\lambda \approx 1.49$ and $\tilde{h} \approx 0.043$). Collision points (+) where two surface modes collide are given by (13) and (14). Crossing a dashed line in the direction of an arrow labelled i leads to an increase in the number of actual surface modes in region $\mathcal{R}_i$.

energy from the fluid and are hence physical, we may map the curve $\mathrm{Re}(Z) = 0$ into the complex σ plane to separate regions of the σ plane that can and cannot contain surface modes.

Figure 2 plots $\mathrm{Re}(\mu) = 0$ and $\mathrm{Re}(Z) = 0$ in the complex Z and σ planes. The parameters used were chosen to correspond to rotor-alone tones in a typical aeroengine at takeoff, with $M = 0.5$, $\omega = 31$ and $m = 24$, with a boundary layer of thickness $\delta = 10^{-3}$ and a tanh boundary layer profile, as used by Rienstra & Vilenski [23],

$$U(r)/M = \tanh\left(\frac{1-r}{\delta}\right) + \big(1 - \tanh(1/\delta)\big)\left(\frac{1+\tanh(1/\delta)}{\delta}r + (1+r)\right)(1-r), \tag{15}$$

with constant density $R(r) \equiv 1$. The boundary layer parameters for this situation are

$$\delta_1 = 6.9315 \times 10^{-4} \qquad \delta_k = 10^{-3} \qquad \delta_s = 10^{-3} \qquad \delta_0 = 0$$
$$\tilde{h} \approx 4.3 \times 10^{-2} \qquad \Delta_k \approx 0.72135 \qquad \delta_s \approx 0.72135 \qquad \Delta_0 = 0$$

For large $|Z|$ there are two actual surface modes present, located in regions $\mathcal{R}_a$ and $\mathcal{R}_b$ of the σ-plane, as shown in figure 2*c*. As Z varies and crosses the lines of $\mathrm{Re}(\mu) = 0$ in figure 2*a,b*, other actual surface modes appear. In total, there are a maximum of two surface modes possible in each of regions $\mathcal{R}_a$ and $\mathcal{R}_c$, and a maximum of one surface mode possible in each of regions $\mathcal{R}_b$ and $\mathcal{R}_d$. In each of regions $\mathcal{R}_a$ and $\mathcal{R}_c$, the two actual surface modes collide for particular values of Z given by (13) and (14). These values of Z, and the corresponding locations in the σ-plane where the collisions occur, are labelled as s_a and s_c in figure 2. If Z were to be varied in a closed loop around one of the collision points in the Z-plane, the two corresponding surface modes in the σ-plane would exchange places. This makes it difficult to consistently label the surface modes. One option, adopted by Ref. 7, would be to introduce a branch cut in the Z-plane from each of these collision points, artificially preventing the two modes from exchanging places. However, no choice of branch cut would give a labelling of the two modes consistent with simultaneously whether the modes exist (as plotted in figure 2) and whether they are stable or unstable (as discussed in section 5), and hence no further labelling is given here.

Since figures 2*a,c* do not look like their equivalent with uniform flow (see, for example, figure 2 of Ref. 7), it is interesting to see how the uniform flow results are recovered in the limit $\tilde{h} \to 0$ by making the boundary layer progressively thinner. Figure 3 shows the comparable diagrams to figures 2*a,c* for the same parameters but for a tanh boundary layer with thicknesses $\delta = 3 \times 10^{-4}$, $\delta = 2.5 \times 10^{-4}$ and $\delta = 5 \times 10^{-5}$, by which time the corresponding $\lambda = 1.5$ solution from figure 2 of Ref. 7 is becoming recognisable.

This section has described the position and number of surface modes for the particular values $\lambda \approx 1.5$, $M = 0.5$, $\tilde{h} \approx 0.043$, and a tanh boundary layer profile. It is not possible to give a complete catalogue of all possible parameter regimes here, as was done in Ref. 7 for the uniform case, owing to the number of free parameters. However, it is expected that the situation described here is indicative of a relatively large and aeroacoustically-useful range of parameters, and the same analysis as used here may be applied without modification to other set of parameters.

4 Numerical comparison

In this section, we consider the frequency ω to be given and solve for the axial wavenumber k. We will compare the predictions of the *modified Myers surface mode* (MMSM) dispersion relation (7), as discussed in the previous section, with a number of progressively less approximate dispersion relations. The first of these is the *Short Wavelength Modified Myers* (SWMM) dispersion relation, consisting of the dispersion relation (3) with Z_{mod} given by (4) and with the short wavelength approximation $\delta I_1 \sim \delta_s M k/\omega$, which is exact for a linear-then-constant boundary layer profile given by (12). Similarly, the *Full Modified Myers* (FMM) dispersion relation is given by (3) with Z_{mod} given by (4) but with the δI_1 integral being computed numerically.

As a check on the accuracy of these approximations, we also consider the dispersion relation given by solving the full Pridmore-Brown equation (1) numerically, since the Pridmore-Brown equation is a direct rearrangement of the linearized Euler equations. The appropriate boundary conditions are regularity of pressure p_m at $r = 0$ and the impedance boundary condition at $r = 1$ (assuming $U(1) = 0$),

$$Z p_m'(1) + \mathrm{i}\omega R(1) p_m(1) = 0. \tag{16}$$

The Pridmore-Brown dispersion relation (labelled PB in the figures) is given by finding the value of k such that (1) subject to these boundary conditions possesses a nonzero solution. Equation (1) is solved using a 12th order implicit central finite difference method, with grid points clustered so as to provide sufficient resolution within even very thin boundary layers (the same code was used for the numerical results of Ref. 13); typically 4000 radial points were used. The boundary condition at $r = 1$ was then satisfied using a Newton-Raphson iteration to find the axial wavenumber k, with iteration starting points chosen close to predicted positions of modes and on an evenly spaced grid to find unpredicted modes.

Since the asymptotics of Brambley [13], leading to the modified Myers boundary condition given in (3) and (4), are based on the Pridmore-Brown equation to first order in the boundary layer thickness, what follows also provides a useful comparison of the accuracy of this boundary condition. For comparison, we also include here the results of the unmodified Myers boundary condition (labelled *Myers* in the figures), given by the dispersion relation (3) with $Z_{\mathrm{mod}} = Z$, and the unmodified surface mode dispersion relation which follows from it [6, 7] (labelled as UMSM in the figures).

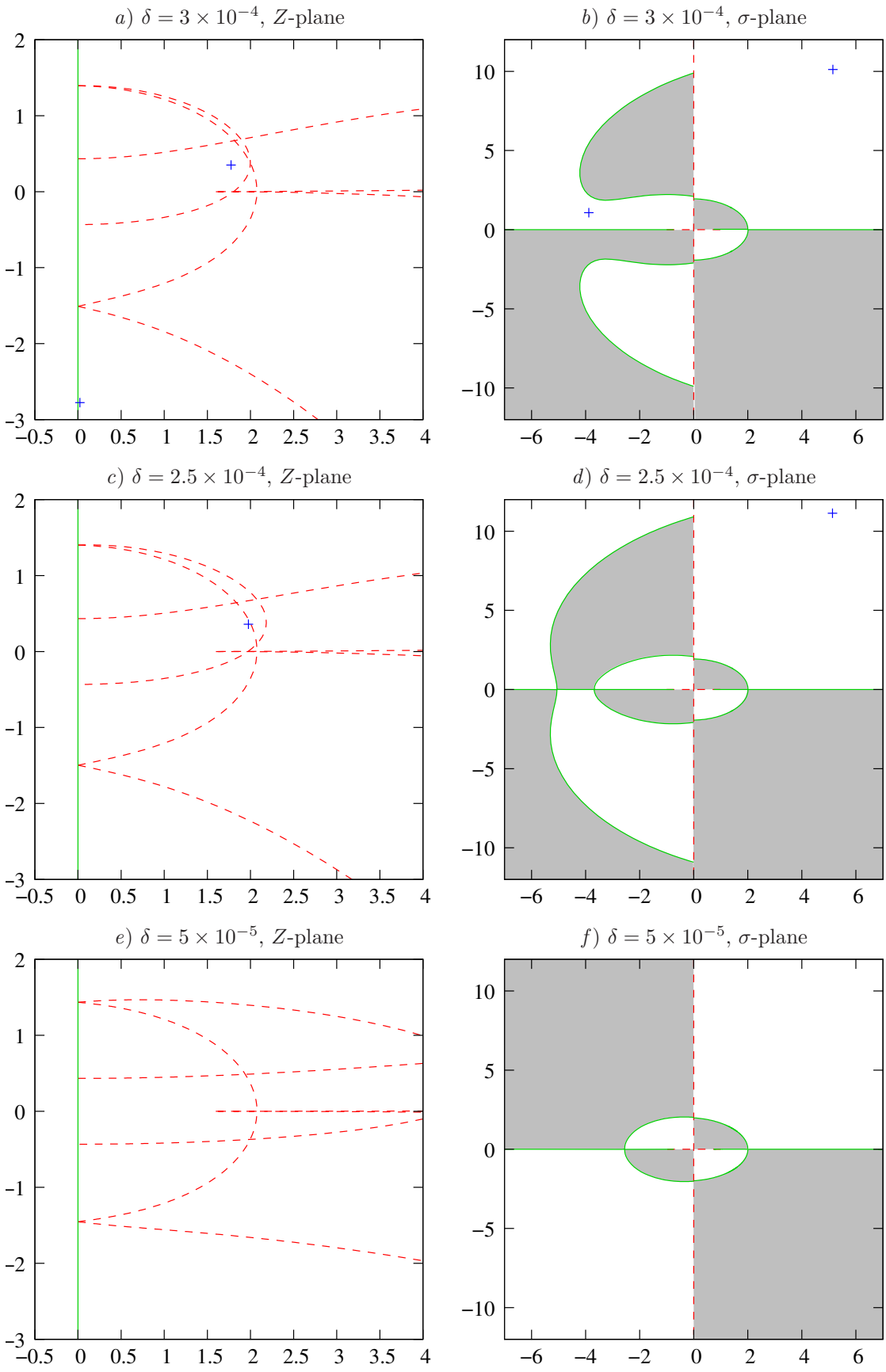

Figure 3: The curves $\mathrm{Re}(Z) = 0$ (solid lines) and $\mathrm{Re}(\mu) = 0$ (dashed lines), and the collision points (+), plotted in the complex Z- and σ-planes for the same parameters as figure 2 but with different boundary layer thicknesses. The boundary layer has a tanh profile given by (15) with thickness δ and $M = 0.5$, for $\omega = 31$ and $m = 24$ (giving $\lambda \approx 1.49$). The collision point in e) and f) at $Z \approx 4.7 + 0.4\mathrm{i}$ and $\sigma \approx 5.1 + 25.1\mathrm{i}$ is not shown owing to the scale used.

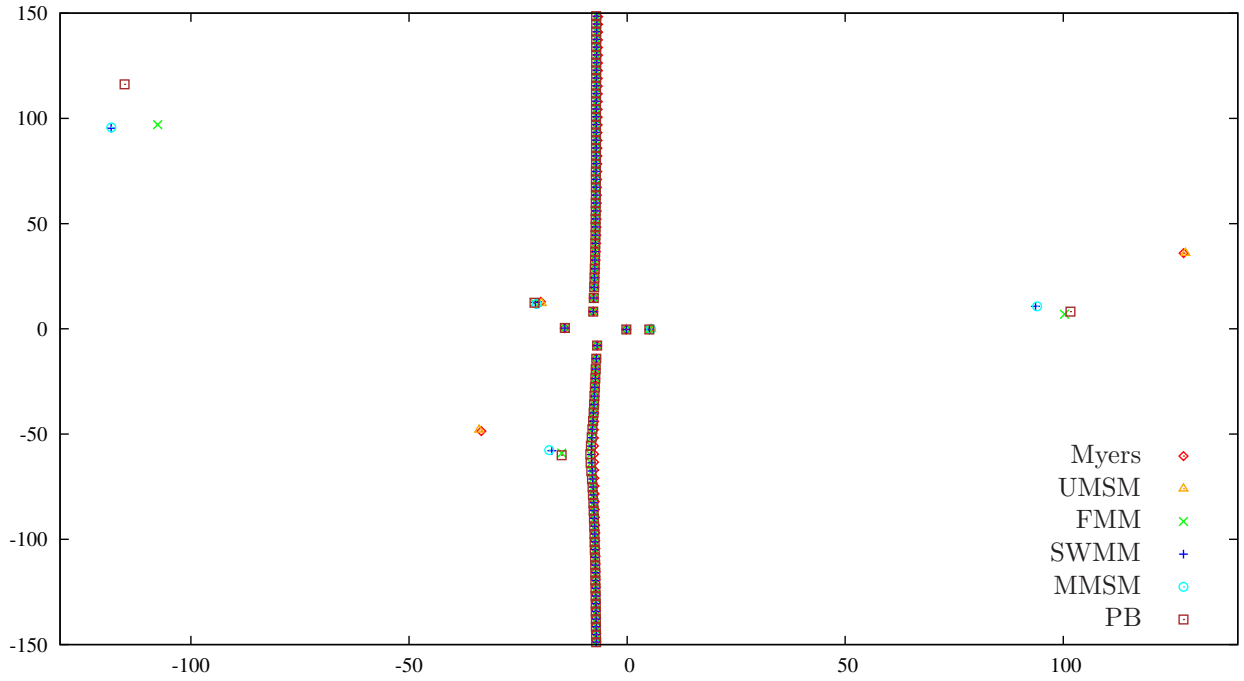

Figure 4: Axial wavenumbers (k) in the complex k-plane for a boundary impedance $Z = 1 - 2.5\mathrm{i}$ and various dispersion relations, for $\omega = 10$, $m = 5$, and a tanh boundary layer profile (15) with $\delta = 10^{-3}$. Dispersion relations: UMSM = Unmodified Myers Surface Mode, FMM = Full Modified Myers, SWMM = Short Wavelength Modified Myers, MMSM = Modified Myers Surface Mode, PB = Pridmore-Brown numerical modes.

We consider here two different sets of parameters, namely $(\omega, m) = (31, 24)$ and $(\omega, m) = (10, 5)$. For most cases here, the boundary layer thickness is 10^{-3} and the centreline Mach number is $M = 0.5$. Two boundary layer profiles are used: the *linear* profile given by (12), with the thickness defined to be h, and the *tanh* profile given by (15), with the thickness defined to be δ; note that this gives $\delta_s = 10^{-3}$ in both cases.

4.1 Comparison of predicted surface mode accuracy

Figure 4 shows the allowable axial wavenumbers for $(\omega, m) = (10, 5)$ with a tanh boundary layer profile and an impedance boundary with $Z = 1 - 2.5\mathrm{i}$. In this case, the modified Myers surface mode (MMSM) dispersion relation (7) correctly predicts the existence and location of five actual surface modes: two in region $\mathcal{R}_c$ (the top-left quadrant of the k-plane) and one in each of regions $\mathcal{R}_a$, $\mathcal{R}_b$ and $\mathcal{R}_d$. The unmodified Myers surface mode (UMSM) dispersion relation predicts only four actual surface modes, of which the locations of only two are predicted accurately. Figure 4 also demonstrates the general features that the best approximation to the exact Pridmore-Brown (PB) numerical solutions is the FMM solution, followed by the more-easily-computed SWMM approximation. The MMSM results, being a surface mode approximation of SWMM, agree almost exactly with the surface modes found using the SWMM method. Similarly, the UMSM results, being a surface mode approximation of the Myers boundary condition, agree almost exactly with the surface modes found using the Myers approximation. These observations continue to be borne out in the following numerical examples.

Figure 5a uses similar parameters to figure 4 but for the impedance $Z = 1.6 + 0.2\mathrm{i}$. In this case, the MMSM approximation correctly predicts the existence of two surface modes in region $\mathcal{R}_a$. This is significant, as UMSM approximation predicts only one in this quadrant, which Rienstra [6] tentatively predicted to be a hydrodynamic instability, and which appears to be confirmed by recent investigations [10, 13]. (In fact, we will see in §5 that one of the two surface modes in this region is indeed an instability, while the other is stable.) A similar plot to figure 5 for the parameters $(\omega, m) = (31, 24)$, motivated by their relevance to rotor-alone noise in an aeroengine intake, is show in figure 6 for $Z = 0.6 - 2\mathrm{i}$. The MMSM approximation correctly predicts the existence of two actual surface modes in region $\mathcal{R}_c$, one in $\mathcal{R}_b$ and none in $\mathcal{R}_d$, while the UMSM approximation incorrectly predict a surface mode in region $\mathcal{R}_d$ and fail to predict the second surface mode in region $\mathcal{R}_c$. However, the most interesting behaviour is seen in region $\mathcal{R}_a$ (the upper-right quadrant of the k-plane). The UMSM approximation predict a surface mode in this region, but inaccurately predict its location, while the MMSM approximation predicts a surface mode much closer to the real k axis; this surface mode, however, is actually only actually

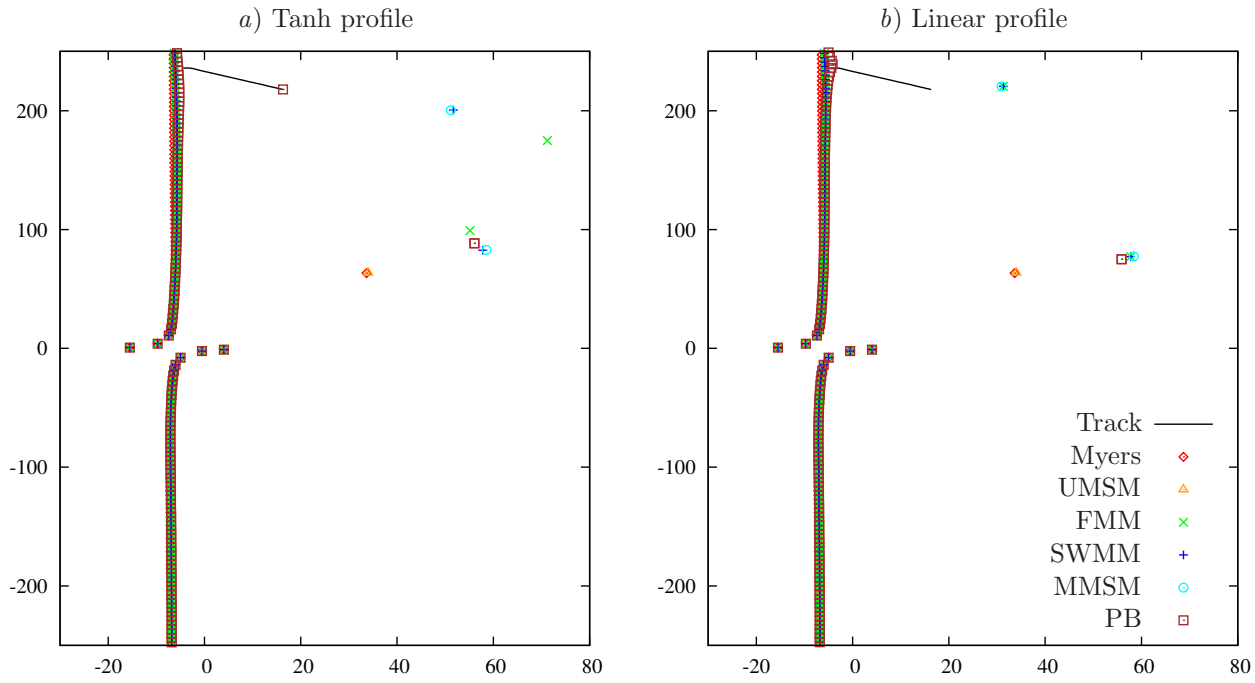

Figure 5: Axial wavenumbers (k) in the complex k-plane for a boundary impedance $Z = 1.6 + 0.2\mathrm{i}$ and various dispersion relations, for $\omega = 10$, $m = 5$, and a) a tanh boundary layer profile (15) with $\delta = 10^{-3}$, and b) a linear boundary layer profile (12) with $h = 10^{-3}$. "Track" refers to the motion of one particular PB numerical mode as the boundary layer profile is smoothly deformed from tanh to linear. Dispersion relations: UMSM = Unmodified Myers Surface Mode, FMM = Full Modified Myers, SWMM = Short Wavelength Modified Myers, MMSM = Modified Myers Surface Mode, PB = Pridmore-Brown numerical modes.

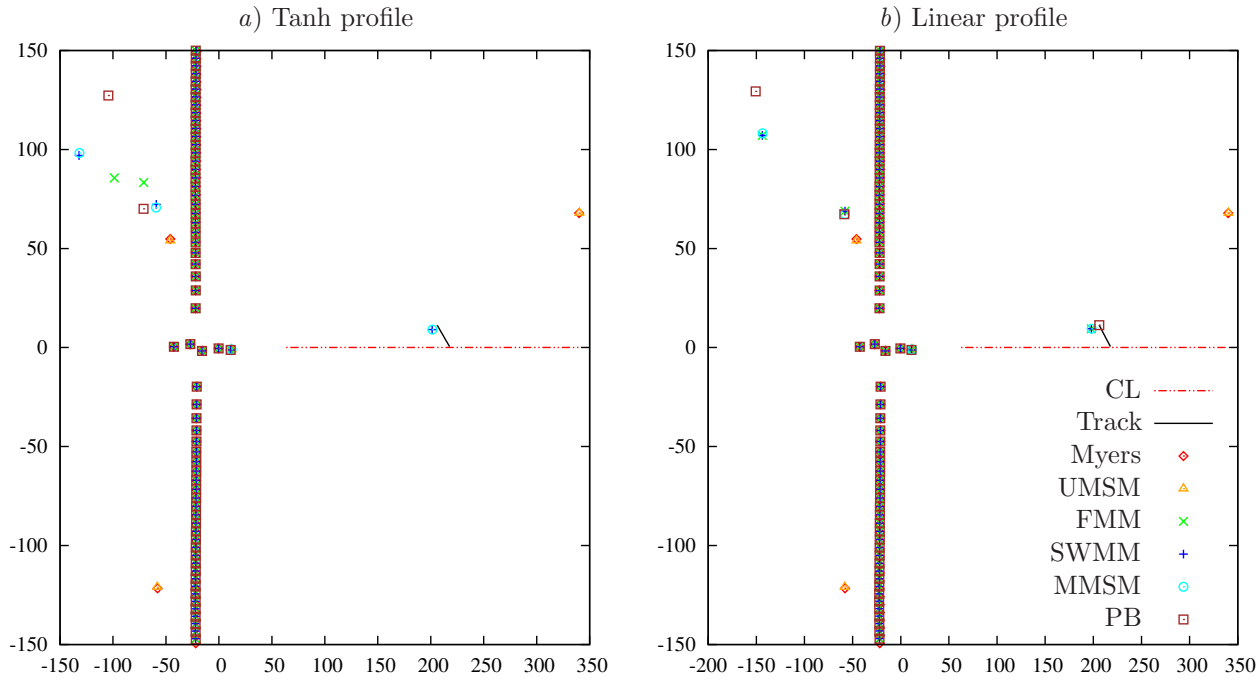

Figure 6: Axial wavenumbers (k) in the complex k-plane for $Z = 0.6 - 2\mathrm{i}$, $\omega = 31$, $m = 24$, and a) a tanh boundary layer profile (15) with $\delta = 10^{-3}$, and b) a linear boundary layer profile (12) with $h = 10^{-3}$. "Track" refers to the motion of one particular PB numerical mode as the boundary layer profile is smoothly deformed from tanh to linear. Dispersion relations: UMSM = Unmodified Myers Surface Mode, FMM = Full Modified Myers, SWMM = Short Wavelength Modified Myers, MMSM = Modified Myers Surface Mode, PB = Pridmore-Brown numerical modes. CL indicates the critical layer branch cut.

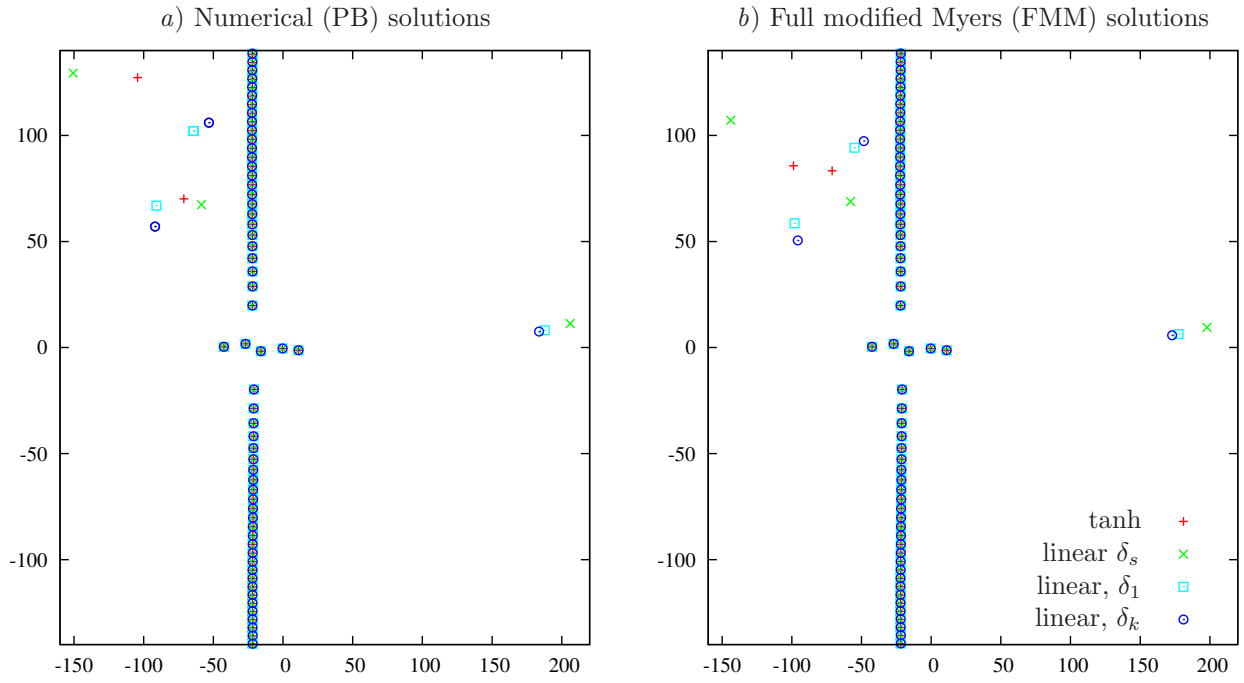

Figure 7: Axial wavenumbers (k) in the complex k-plane for four different boundary layers: a tanh profile with $\delta = 10^{-3}$, a linear profile with $h = 10^{-3}$ (matching the δ_s of the tanh profile), a linear profile with $h = 1.39 \times 10^{-3}$ (matching the δ_1 of the tanh profile), and a linear profile with $h = 1.5 \times 10^{-3}$ (matching the δ_k of the tanh profile). a) numerical solutions to the Pridmore-Brown equation (labelled PB in figure 6); b) full modified Myers solutions (labelled FMM in figure 6). Other parameters are as for figure 6: $M = 0.5$, $\omega = 31$, $m = 24$, and $Z = 0.6 - 2\mathrm{i}$.

present for a linear boundary layer profile (as shown by the numerical PB results), and is not present for the tanh boundary layer profile. Motivated by this difference, we next investigate the effect of the boundary layer profile.

4.2 Comparison of tanh and linear boundary layer profiles

Figures 5a and 5b compare respectively a tanh and linear boundary layer profile for $(\omega, m) = (10, 5)$ and $Z = 1.6 + 0.2\mathrm{i}$. For the linear boundary layer profile, the δI_1 short wavelength approximation (4c) becomes exact, and so the FMM and SWMM results coincide for a linear boundary layer profile. While the surface modes (both numerically-calculated and predicted) move a moderate amount when the boundary layer profile is changed, what is most striking is that there is one surface mode in region $\mathcal{R}_a$ (the upper-right quadrant of the k-plane) that is present for the tanh case (figure 5a) and not present for the linear case (figure 5b), despite all the approximations predicting it to be present in both cases. The track taken by this mode as the flow velocity $U(r)$ is linearly interpolated between the tanh and linear profiles is shown in both figures 5a and b, clearly demonstrating that this mode has disappeared and become an ordinary cut-off acoustic mode, and eliminating the possibility that the numerics has failed to find this mode for the linear profile.

Figures 6a and 6b similarly compare a tanh and linear boundary layer profile for $(\omega, m) = (31, 24)$ and $Z = 0.6 - 2\mathrm{i}$. In this case the MMSM and SWMM approximations predict a surface mode close to the real k axis, which in fact is only actually present for a linear boundary layer profile (as seen by the numerical PB solution). Tracking this mode as the mean velocity $U(r)$ is linearly varied from a linear to a tanh profile shows that this mode disappears behind the critical layer branch cut located on the real k axis (see Ref. 16 for further details of the critical layer). Note that the FMM results also predict the same behaviour as the PB results.

The tanh profile used in figures 5 and 6 has $\delta_0 = 0$, $\delta_1 \approx 7 \times 10^{-4}$, $\delta_k = 10^{-3}$ and $\delta_s = 10^{-3}$, while the linear profile used in these figures has $\delta_0 = 0$, $\delta_1 = 5 \times 10^{-4}$, $\delta_k \approx 7 \times 10^{-4}$ and $\delta_s = 10^{-3}$. One might think, therefore, that the differences between the linear- and tanh-profiles are due to the two boundary layer profiles have different effective thicknesses. However, figure 7 compares the numerical Pridmore-Brown modes (figure 7a) and the Full Modified Myers approximation (figure 7b) for a tanh boundary layer profile with $\delta = 10^{-3}$ and linear profiles with $h = 10^{-3}$, $h = 1.39 \times 10^{-3}$, and $h = 1.5 \times 10^{-3}$; these three linear profiles match respectively the δ_s, δ_1 and δ_k values of the tanh profile. While it is interesting to note the significant variation of the surface modes in region

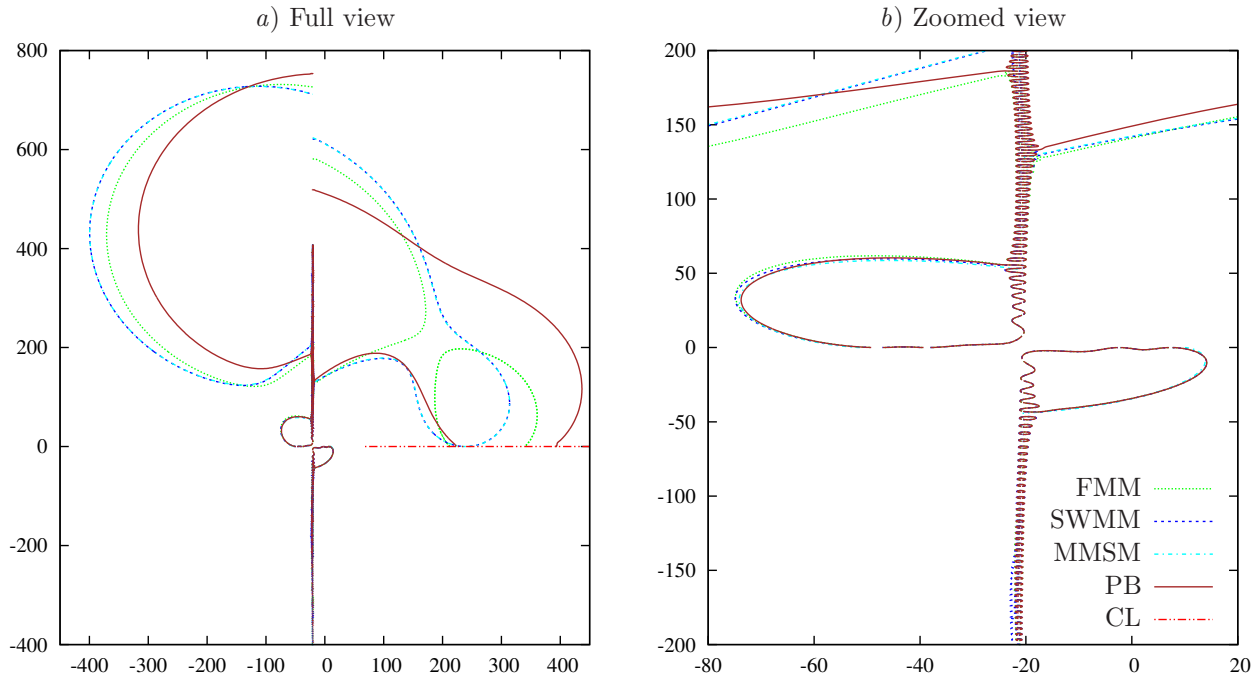

Figure 8: Trajectories of axial wavenumbers (k) in the complex k-plane as $\mathrm{Im}(Z)$ is varies with $\mathrm{Re}(Z) = 0.75$. Parameters are as for figure 6: a tanh boundary layer profile with $\delta = 10^{-3}$ and $M = 0.5$, with $\omega = 31$ and $m = 24$. Solutions are for FMM = Full Modified Myers, SWMM = Short Wavelength Modified Myers, MMSM = Modified Myers Surface Mode, and PB = Pridmore-Brown numerical modes, with CL labelling the critical layer branch cut.

$\mathcal{R}_c$ (the upper-left quadrant of the k-plane), for both the numerical PB solution and the FMM approximation all three linear profiles support a surface mode in region $\mathcal{R}_a$ (the upper-right quadrant of the k-plane) while the tanh profile does not. This demonstrates that the shape of the boundary layer profile can have an important effect on the presence or absence of this unstable surface mode.

4.3 The effect of varying reactance

Here, as considered by, for example, Vilenski & Rienstra [24], we consider the motion of modes as the reactance $\mathrm{Im}(Z)$ varies with the resistance $\mathrm{Re}(Z)$ fixed. This is the typical situation that occurs with, for example, a Helmholtz Resonator impedance [25] where $\mathrm{Re}(Z)$ is fixed and $\mathrm{Im}(Z)$ varies strongly with frequency and tuning parameters (such as the depth of the resonator cell). Figure 8 shows such a situation with $\mathrm{Re}(Z) = 0.75$, again for the parameters $(\omega, m) = (31, 24)$. The value of $\mathrm{Re}(Z) = 0.75$ was chosen to demonstrate a range of behaviours of surface modes, informed by figure 2; for example, this range of Z passes close to both collision points in figure 2*a*. Of the five surface modes shown in figure 8, the two closest to the origin are accurately predicted by all methods. The surface mode in the $\mathcal{R}_c$ region (the upper-left of the k-plane) is notably less accurately predicted, though is still arguably well-predicted quantitatively. In the $\mathcal{R}_a$ region (the upper-right quadrant of the k-plane), one surface mode is accurately predicted and the other is qualitatively well predicted by both the surface mode dispersion relation (7) and the short wavelength modified Myers dispersion relation, both of which agree very closely with one another. However, both of these methods fail to predict the disappearance of these surface modes behind the critical layer branch cut — a feature demonstrated by the numerical Pridmore-Brown solution and also captured by the full modified Myers boundary condition. This shows that the δI_1 integral is strongly connected with the behaviour of the critical layer branch cut, as predicted in Ref. 13. The fact that the full modified Myers solution and the numerical Pridmore-Brown solution show different trends in the upper-right k-plane is explained by the close proximity of collision point s_a in figure 2, which the full modified Myers solution has placed on the wrong side of the line $\mathrm{Re}(Z) = 0.75$.

4.4 Results for thicker boundary layers

All the results above have involved a relatively thin boundary layer of thickness of the order of 10^{-3}. Figure 9 compares the motion of the modes of the full modified Myers and the numerical Pridmore-Brown dispersion

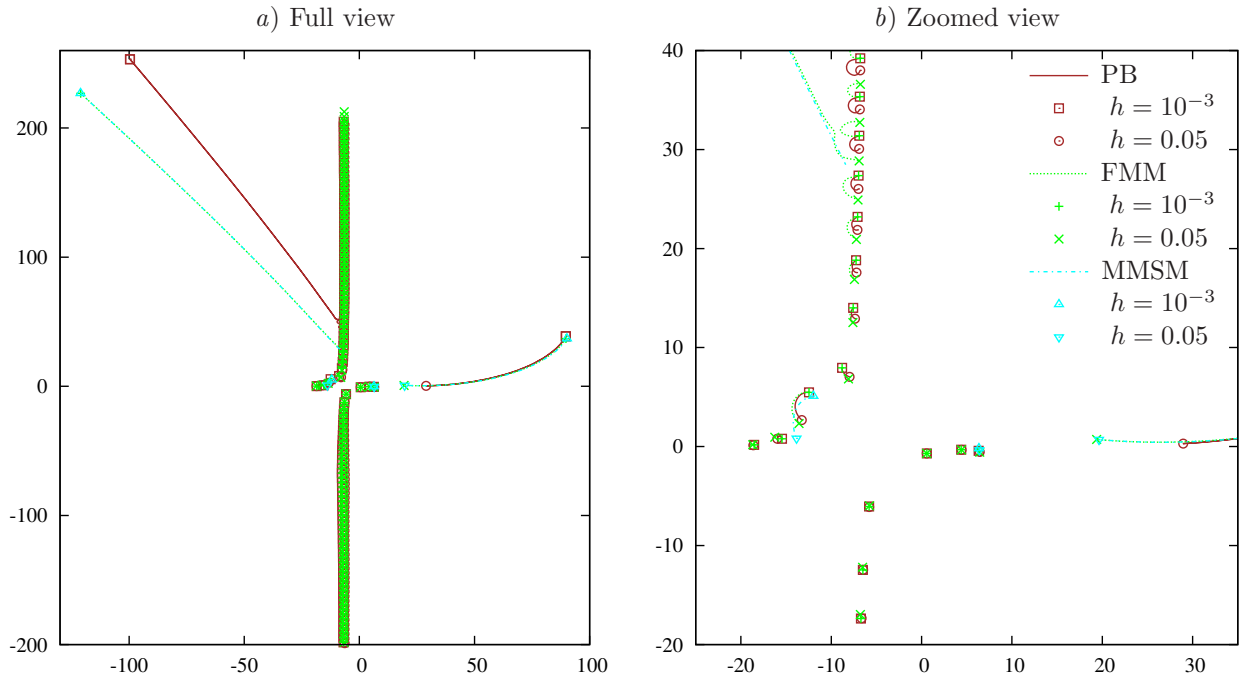

Figure 9: Motion of modes in the complex k-plane for a linear boundary layer profile with $h \in [0.001, 0.05]$, $M = 0.5$, $\omega = 10$, $m = 2$, and $Z = 2 - \mathrm{i}$. Dispersion relations: PB = Pridmore-Brown numerical modes, FMM = full modified Myers, MMSM = Modified Myers Surface Mode.

relations to the surface mode prediction of (7) for a linear boundary layer profile as the thickness is varied for $10^{-3} \leq h \leq 0.05$, for $(\omega, m) = (10, 2)$ and $Z = 2 - \mathrm{i}$, enabling comparison with Ref. 16. Indeed, figure 9 supports Ref. 16 by demonstrating that, while four surface modes are supported for these parameters for a thin boundary layer with $h = 10^{-3}$ (two in region $\mathcal{R}_c$, and one each in regions $\mathcal{R}_a$ and $\mathcal{R}_b$), only three survive for $h = 0.05$. Moreover, the instability surface mode in region $\mathcal{R}_a$ moves along and very close to the critical layer branch cut as the boundary layer is thickened, in line with the findings of Ref. 16. The instability found in Ref. 16 may therefore be identified with the unstable surface mode in region $\mathcal{R}_a$.

5 Stability

Dispersion relations such as (7) may be solved for k given ω, corresponding to the boundary value problem of sound generated by an oscillator of frequency ω at a particular axial location, or may be solved for ω given k, corresponding to the initial value problem of the temporal evolution of an initial perturbation of axial wavelength $2\pi/k$. In the latter case, usually k is real (corresponding to a bounded initial perturbation), and $-\mathrm{Im}(\omega(k))$ gives the exponential temporal growth rate of an initial perturbation of wavenumber k. The maximum temporal growth rate, $-\min_k(\mathrm{Im}(\omega(k)))$, is also important for a Briggs–Bers [20, 21] stability analysis, similar to that performed in Ref. 13. This stability analysis involves smoothly varying ω, with the imaginary part going from being large and negative to zero with the real part held fixed; modes are considered to be left-propagating (upstream propagating) if they originate in the upper-half k-plane for negative $\mathrm{Im}(\omega)$, and right-propagating (downstream propagating) if they originate in the lower-half k-plane. As described, for example, in Ref. 8, this deformation is because the initial contour $\mathcal{C}_\omega$ along which an $\omega \to t$ Fourier inversion should be performed must be taken below all roots of the dispersion relation $\omega(k)$ for real k in order to satisfy causality. We first consider the surface mode approximations for $\omega(k)$ for real k, before then searching for absolute and convective instabilities using a Briggs–Bers stability analysis.

5.1 Temporal instability

In this section, we investigate $\omega(k)$ asymptotically for the surface modes, with an emphasis on temporally-unstable modes for which $\mathrm{Im}(\omega) < 0$. We assume that $\omega/k \ll 1$, $m/k \ll 1$, $k\delta \ll 1$, and that the impedance Z is locally reacting (so that Z contains no k dependence) and at least mass like at high frequencies (so that $|\omega/Z|$

is bounded as $|\omega| \to \infty$). Then, using the approximation

$$\sqrt{k^2+m^2-(\omega-Mk)^2} = \pm\big(\beta\Lambda k + M\omega/\beta\big) + kO\big(\omega^2/k^2, m^4/k^4\big), \qquad \text{where} \qquad \Lambda = \left(1+\frac{m^2}{2\beta^2k^2}\right) \tag{17}$$

and $\pm = \mathrm{sgn}(\mathrm{Re}(k))$, the leading and first order terms in the surface mode dispersion relation (7) turn out to be

$$\mp\big(\beta\Lambda k\omega + M\omega^2/\beta\big)\big(\mathrm{i}\omega Z + M^2k^2\delta_k\big) + M^2k^2\omega - 2Mk\omega^2 + \mathrm{i}\omega Z\delta_s Mk\big(k^2{+}m^2\big) = 0. \tag{18}$$

Under the assumptions about Z given above, to leading order in ω/k equation (18) is

$$\mathrm{i}\omega Z\Big(\delta_s M\big(k^2{+}m^2\big) \mp \beta\Lambda\omega\Big) + M^2k\omega = 0. \tag{19}$$

Balancing these three terms gives the distinguished scaling

$$k \sim \mathrm{i}\omega Z \qquad\qquad \omega \sim \delta_s k^2, \tag{20}$$

from which it may be checked that (18) is indeed correct to leading and first order. Rearranging (19) gives

$$\mp\mathrm{i}\omega Z M\omega^2/\beta = \frac{-\mathrm{i}\omega Z\delta_s M^2\omega\big(k^2{+}m^2\big)}{\Lambda\beta^2} - \frac{M^3k\omega^2}{\Lambda\beta^2}, \tag{21}$$

meaning that (18) may be rewritten, still correct to first order in ω/k, as

$$\mp\beta\Lambda\omega\big(\mathrm{i}\omega Z + M^2k^2\delta_k\big) + M^2k\omega - 2M\omega^2 + \mathrm{i}\omega Z\delta_s M\big(k^2{+}m^2\big) - \frac{\mathrm{i}\omega Z\delta_s M^2\omega\big(k^2{+}m^2\big)}{k\Lambda\beta^2} - \frac{M^3\omega^2}{\Lambda\beta^2} = 0. \tag{22}$$

While (22) is valid for any impedance that is at least mass-like for large frequencies, to progress further we must choose a model for the impedance Z. The model chosen here is the commonly-used mass–spring–damper model,

$$\mathrm{i}\omega Z = -d\omega^2 + b + \mathrm{i}\mathcal{R}\omega. \tag{23}$$

Expanding (22) then gives a cubic polynomial for ω,

$$\begin{aligned}\left(\pm d\beta\Lambda + \frac{d\delta_s M^2\big(k^2{+}m^2\big)}{k\Lambda\beta^2}\right)\omega^3 + \left(-d\delta_s M\big(k^2{+}m^2\big) - 2M - \frac{M^3}{\Lambda\beta^2} \mp \beta\Lambda\mathrm{i}\mathcal{R} - \frac{\mathrm{i}\mathcal{R}\delta_s M^2\big(k^2{+}m^2\big)}{k\Lambda\beta^2}\right)\omega^2 \\ + \left(M^2k \mp \beta\Lambda b - \frac{b\delta_s M^2\big(k^2{+}m^2\big)}{k\Lambda\beta^2} \mp \beta\Lambda M^2k^2\delta_k + \mathrm{i}\mathcal{R}\delta_s M\big(k^2{+}m^2\big)\right)\omega + b\delta_s M\big(k^2{+}m^2\big) = 0.\end{aligned} \tag{24}$$

The predictions of (24) are investigated in §5.2, and an example is shown in figure 10. For this mass–spring–damper impedance, equation (20) gives two scalings. For the first scaling, $\omega \ll 1$, so that $\mathrm{i}\omega Z \sim O(1)$ and (20) gives $k \sim O(1)$ and $\omega \sim O(\delta_s)$. This case is reasonably uninteresting, with (24) reducing to the quadratic equation in ω,

$$\left(\mp\mathrm{i}\mathcal{R}\beta\Lambda - 2M \mp \frac{bM}{\beta k}\right)\omega^2 + \Big(\mp b\beta\Lambda + M^2k \mp \beta\Lambda M^2k^2\delta_k + \mathrm{i}\mathcal{R}\delta_s M\big(k^2{+}m^2\big)\Big)\omega + b\delta_s M\big(k^2{+}m^2\big) = 0. \tag{25}$$

The range of k for which this solution is accurate is rather small, and this solution is included here only for completeness. The second scaling, $\omega \gg 1$, is the most useful for stability analysis. In this case, since $\mathrm{i}\omega Z \sim O(\omega^2)$, equation (20) gives $\omega \sim O({\delta_s}^{-1/3})$ and $k \sim O({\delta_s}^{-2/3})$, so that (22) becomes a quadratic equation for ω,

$$\begin{aligned}\big(\pm d\beta + d\delta_s M^2k/\beta^2\big)\omega^2 + \big(-d\delta_s Mk^2 - 2M - M^3/\beta^2 \mp \beta\mathrm{i}\mathcal{R} - \mathrm{i}\mathcal{R}\delta_s M^2k/\beta^2\big)\omega \\ + \big(M^2k \mp \beta M^2k^2\delta_k + \mathrm{i}\mathcal{R}\delta_s Mk^2\big) = 0,\end{aligned} \tag{26}$$

where, since only terms of order $O({\delta_s}^{-2/3})$ and $O({\delta_s}^{-1/3})$ have been retained, no m-dependence remains. Note that, strictly speaking, the term $\omega\mathrm{i}\mathcal{R}\delta_s M^2k/\beta^2$ should also have been omitted since it is $O(1)$, although here we retain this term since it turns out to lead to fortuitous behaviour when $k{\delta_s}^{-2/3}$ becomes larger.

The cubic and quadratic approximations (24) and (26) are compared to a full numerical solution of the Pridmore-Brown equation, the modified Myers boundary condition and the surface mode approximation in figure 10, showing the curves of $\omega(k)$ for real k for a mass–spring–damper impedance for the two cases of a

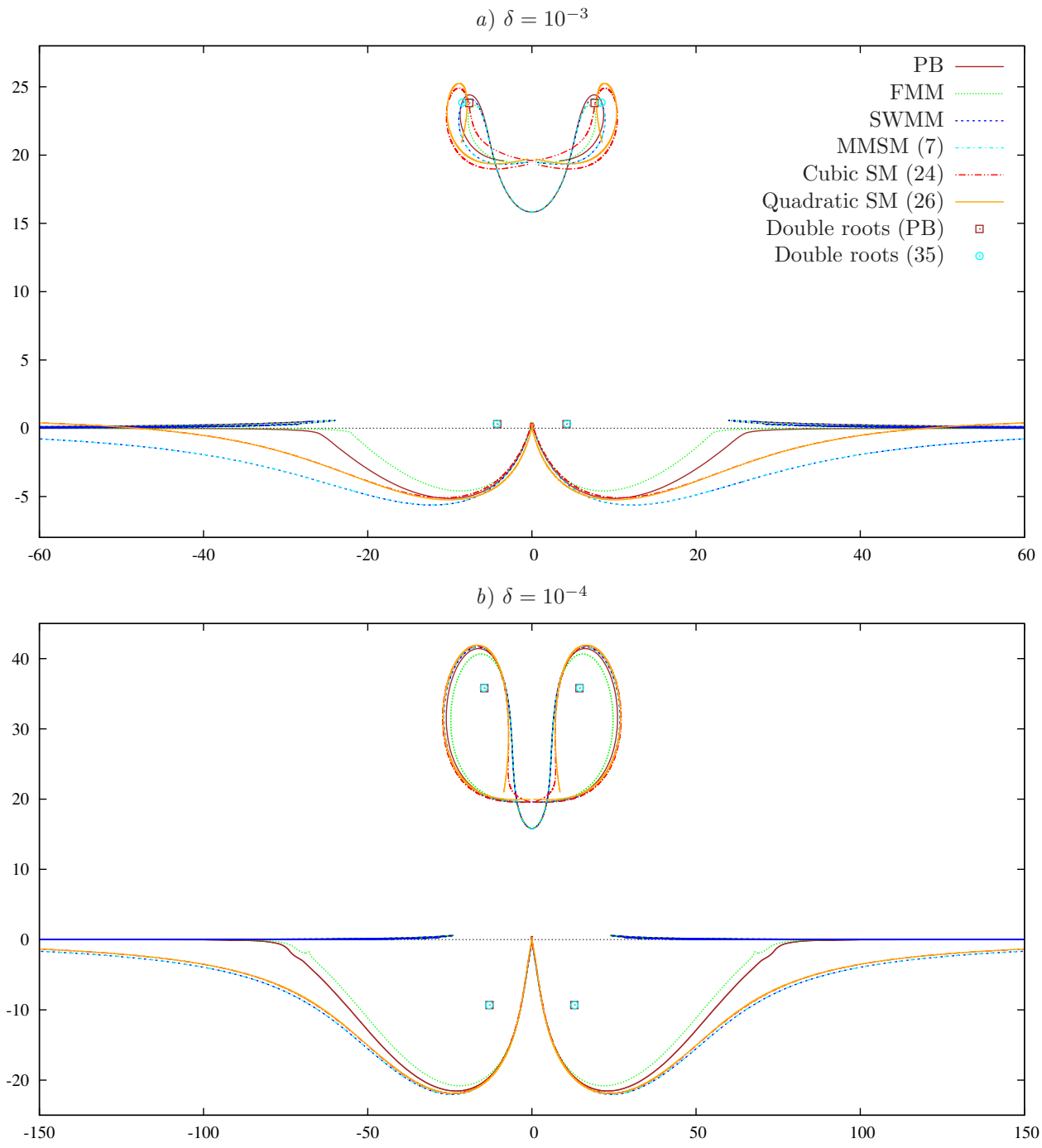

Figure 10: Trajectories of modes in the complex ω-plane for real k, for $m = 24$, a mass–spring–damper impedance $Z = 3 + 0.15\mathrm{i}\omega - 1.15\mathrm{i}/\omega$, and a tanh boundary layer profile given by (15) with $M = 0.5$ and *a*) $\delta = 10^{-3}$ or *b*) $\delta = 10^{-4}$. Dispersion relations: PB = Pridmore-Brown numerical solution, FMM = Full Modified Myers, SWMM = Short Wavelength Modified Myers, MMSM = Modified Myers Surface Mode, SM = Surface Mode.

tanh boundary layer profile with $\delta = 10^{-3}$ and $\delta = 10^{-4}$. As can be seen, both (24) and (26) give a good qualitative agreement with the more exact methods in both cases, while also giving a good quantitative match with the short wavelength modified Myers solution they are approximating in the $\delta = 10^{-4}$ case. Note that the qualitative agreement in figure 10*a* is surprisingly good considering that the asymptotically-small parameter used to derive (26) is ${\delta_s}^{1/3} = 0.1$, which in this case is of the same order as the assumed $O(1)$ quantity $d/b \approx 0.13$.

We now consider the maximum temporal growth rate $-\min_k(\mathrm{Im}(\omega(k)))$ for real k. To leading order (26) gives the two roots,

$$\omega = \frac{\delta_s M k|k|}{2\beta} \pm \frac{\mathrm{i}M}{2\beta}\sqrt{4\beta|k|/d - {\delta_s}^2 k^4}. \tag{27}$$

Choosing k such that $\mathrm{dIm}(\omega)/\mathrm{d}k = 0$ gives a prediction for the maximum temporal exponential growth rate,

$$\mathrm{Im}(\omega_{\max}) \sim \frac{-M\sqrt{3}}{2\left(\delta_s \beta d^2\right)^{1/3}} \qquad \mathrm{Re}(\omega_{\max}) \sim \frac{\pm M}{2\left(\delta_s \beta d^2\right)^{1/3}} \qquad k_{\max} \sim \pm\left(\frac{\beta}{d{\delta_s}^2}\right)^{1/3}. \tag{28}$$

In practice, (28) tends to over-predict $-\mathrm{Im}(\omega_{\max})$, and hence it provides a sufficient value to take for $\mathrm{Im}(\omega)$ during a Briggs–Bers stability analysis. For example, in figure 10*a*, Briggs–Bers trajectories starting from $\mathrm{Im}(\omega) = -5.7$ would be sufficient to ascertain the convective stability of the modes, while (28) gives the approximate lower bound $\mathrm{Im}(\omega) \approx -16.1$. In figure 10*b*, trajectories starting from $\mathrm{Im}(\omega) = -22.1$ would be sufficient, while (28) gives the approximate lower bound $\mathrm{Im}(\omega) \approx -34.7$. Note that (28) also shows: that the relevant boundary layer thickness for stability is δ_s; that the relevant impedance parameter is the mass of the boundary d; that the growth rate is proportional to the Mach number of the mean flow for low to medium subsonic Mach numbers; and that increasing the mass of the boundary could be used to counter the destabilizing effect of a thin boundary layer. Moreover, (28) suggests that for any parameters there will always be a surface mode for which $\mathrm{Im}(\omega(k)) < 0$ for some real values of k, and that at the most negative value of $\mathrm{Im}(\omega(k))$ it will have $\mathrm{d}\omega/\mathrm{d}k \sim M(\beta^2 d^2/\delta_s)^{-1/3} > 0$. Hence, for any value of ω underneath the curve $\omega(k)$ for real k, the corresponding surface mode will be in the lower-half k-plane, and for any ω above the curve $\omega(k)$ for real k, the corresponding surface mode will be in the upper-half k-plane. This strongly suggests that for real $\omega > 0$, one of the surface modes in the upper-right k-plane (the $\mathcal{R}_a$ region) is always convectively unstable for any parameters, adding weight to the original tentative classification of a surface mode in this region as a hydrodynamic instability by Rienstra [6]. This conclusion will be backed up with numerical evidence for specific examples in §5.3.

5.1.1 Asymptotics for other impedance models

In deriving (24)–(28), the impedance $Z(\omega)$ has been assumed to be of a mass–spring–damper type (23). The same analysis could be repeated for other impedance models provided the impedance is expressed as a sum of powers of ω (possibly including negative powers), and so for more complex impedances a Laurent expansion could be used about a particular frequency of interest; however, the analysis would be significantly more complicated if $\mathrm{i}\omega Z$ were to contain more terms than the mass–spring–damper model.

An alternative is to asymptotically expand $Z(\omega)$ for $\mathrm{Im}(\omega) \ll 0$, as this is the range of interest for temporal and absolute instability. For example, consider the Helmholtz resonator impedance model [25] of the form

$$Z(\omega) = \mathcal{R} + \mathrm{i}\omega d L - \mathrm{i}\cot(\omega L), \tag{29}$$

where d is the added mass of the facing sheet nondimensionalized by the mean flow centreline density and the resonator depth, and L is the resonator depth nondimensionalized by the duct radius. For $\mathrm{Im}(\omega) \ll 0$, equation (29) reduces to

$$Z(\omega) \sim \mathcal{R} + 1 + \mathrm{i}\omega d L + O\left(\mathrm{e}^{2\,\mathrm{Im}(\omega L)}\right), \tag{30}$$

so that the temporal stability of flow over a Helmholtz resonator impedance boundary given by (29) may be approximated by (24)–(28) by substituting dL for d, $R+1$ for R, and setting $b = 0$.

5.2 Absolute instability

An absolute instability, being an instability which grows exponentially in time at all spatial locations, is given by a value of ω such that solving the dispersion relation for k gives a double root. In this section, we investigate values of ω leading to a double-root in k of the asymptotic surface mode dispersion relation (18). First, assuming $m^2/k^2 \ll 1$, to leading order (18) gives

$$\mathrm{i}\omega Z \delta_s M k^3 + M^2 \omega k^2 \mp \beta\omega \mathrm{i}\omega Z k = 0, \tag{31}$$

which may be rearranged to give

$$\frac{\mp\omega \mathrm{i}\omega Z m^2}{2\beta k} = -\frac{\mathrm{i}\omega Z \delta_s M m^2 k}{2\beta^2} - \frac{M^2 m^2 \omega}{2\beta^2}. \tag{32}$$

Substituting (32) into (18) and expanding to leading and first order gives the dispersion relation

$$a_3 k^3 + a_2 k^2 + a_1 k + a_0 = 0, \tag{33}$$

where

$$a_3 = \mathrm{i}\omega Z\delta_s M \mp \beta\omega M^2\delta_k \qquad a_2 = M^2\omega$$
$$a_1 = \mp\beta\omega\mathrm{i}\omega Z - 2M\omega^2 + \mathrm{i}\omega Z\delta_s M m^2\left(1-\frac{1}{2\beta^2}\right) \qquad a_0 = \mp\frac{M\omega^2\mathrm{i}\omega Z}{\beta} - \frac{M^2m^2\omega}{2\beta^2}. \tag{34}$$

We now solve simultaneously (33) and the equation $3a_3k^2 + 2a_2k + a_1 = 0$ obtained from differentiating (33) with respect to k. Combining these two equations and eliminating k finally leads to the condition on ω that

$$\left(4a_3a_1^2 - a_2^2a_1 - 3a_3a_0\right)\left(a_2a_1 - 9a_3a_0\right) + \left(6a_3a_1 - 2a_2^2\right)^2 a_0 = 0, \qquad \text{giving} \qquad k = \frac{a_2a_1 - 9a_3a_0}{6a_3a_1 - 2a_2^2}. \tag{35}$$

For a mass–spring–damper impedance (23), after cancellation equation (35) is a polynomial in ω of degree 13 for $m \neq 0$ and of degree 10 for $m = 0$. However, not all of the double roots given by (35) represent absolute instabilities; only double roots with $\mathrm{Im}(\omega) < 0$ for which one of the colliding modes originates in the lower-half k-plane and the other originates in the upper-half represent absolute instabilities, as they pinch the k-Fourier inversion contour (see Ref. 8 for details). Figure 10 plots such double roots given by (35) alongside double roots calculated numerically using the Pridmore–Brown equation, which can be seen to correspond closely in both figures 10*a,b*. In figure 10*b*, two double roots are present with $\mathrm{Im}(\omega) < 0$, and therefore this situation is absolutely unstable, while in figure 10*a*, the two double roots satisfy $\mathrm{Im}(\omega) > 0$ and therefore correspond to exponentially decaying disturbances. For the parameters used in figure 10, the critical thickness for which these double roots have $\mathrm{Im}(\omega) = 0$ is found using the Pridmore–Brown numerical solution to be $\delta = 8.474 \times 10^{-4}$, occurring at $\omega = 4.678$ and $k = 26.77 + 93.93\mathrm{i}$, while the approximation (35) gives $\delta = 8.260 \times 10^{-4}$ occurring at $\omega = 4.822$ and $k = 31.26 + 89.30\mathrm{i}$. These double roots were also found in Ref. 13; the fact that they are well predicted by the polynomial (35) shows that these double roots involve the collision of two *surface modes* in the k-plane, which turn out to be the two surface modes in region $\mathcal{R}_a$ (the upper-right quadrant of the k-plane).

5.3 Convective instability

Here, we consider the convective stability of the various surface modes by smoothly varying $\mathrm{Im}(\omega)$ with $\mathrm{Re}(\omega)$ fixed. In this section a Helmholtz resonator impedance model (29) is used with $d = 4/7$ (as in Refs. 10 and 13), with the cavity depth L varied to give the required impedance at the given frequency. We take $\mathrm{Im}(\omega) = -100$ as the starting point for the Briggs–Bers deformation, although (28) together with (30) indicates that $\mathrm{Im}(\omega) = -62$ would have been sufficient for all examples shown here. It should be remembered that in addition to this convective instability analysis, we must also consider the possibility of an absolute instabilities which, if present, would dominate any convective instability at large times.

Figure 11 shows the Briggs–Bers trajectories as $\mathrm{Im}(\omega)$ is varied from -100 to 0 with $\mathrm{Re}(\omega) = 10$ fixed, for the same parameters as figure 4. Four of the five surface modes and all the acoustic modes are seen to be stable, with the surface mode in region $\mathcal{R}_a$ (the upper-right quadrant of the k-plane) being a downstream-propagating convective instability, as expected. This is in line with Refs. 6, 10 and 13, and also with the observations of Ref. 16 for thicker linear boundary layers.

Figure 12 shows the Briggs–Bers stability analysis for the modes in figure 5*a*. This figure shows the lower surface mode in region $\mathcal{R}_a$ (the upper-right quadrant of the k-plane) as being a downstream-propagating convective instability and the other surface mode as being an upstream-propagating stable mode. However, note that a small change in either the impedance model or parameters could cause $Z(\omega)$ to pass the other side of the the collision point in the complex Z-plane (similar to collision point s_a in figure 2) which would cause the two $\mathcal{R}_a$ surface modes to exchange places, swapping their stability. As mentioned previously, this make it difficult to identify which of these two surface modes is unstable in general without resorting to this stability analysis in each case.

Even more confusingly, figure 13 shows the Briggs–Bers stability analysis for the modes in figure 6*a*. In this case, for the full modified Myers and the numerical Pridmore-Brown dispersion relations, the surface mode in region $\mathcal{R}_a$ is hidden behind the branch cut, while for the short wavelength modified Myers dispersion relation and the modified Myers surface mode dispersion relation this surface mode would be predicted to be a downstream-propagating convective instability. Note that this surface mode does exist if the boundary layer profile is taken as linear (see figure 7), and in this case a similar analysis shows this surface mode to be a downstream-propagating convective instability.

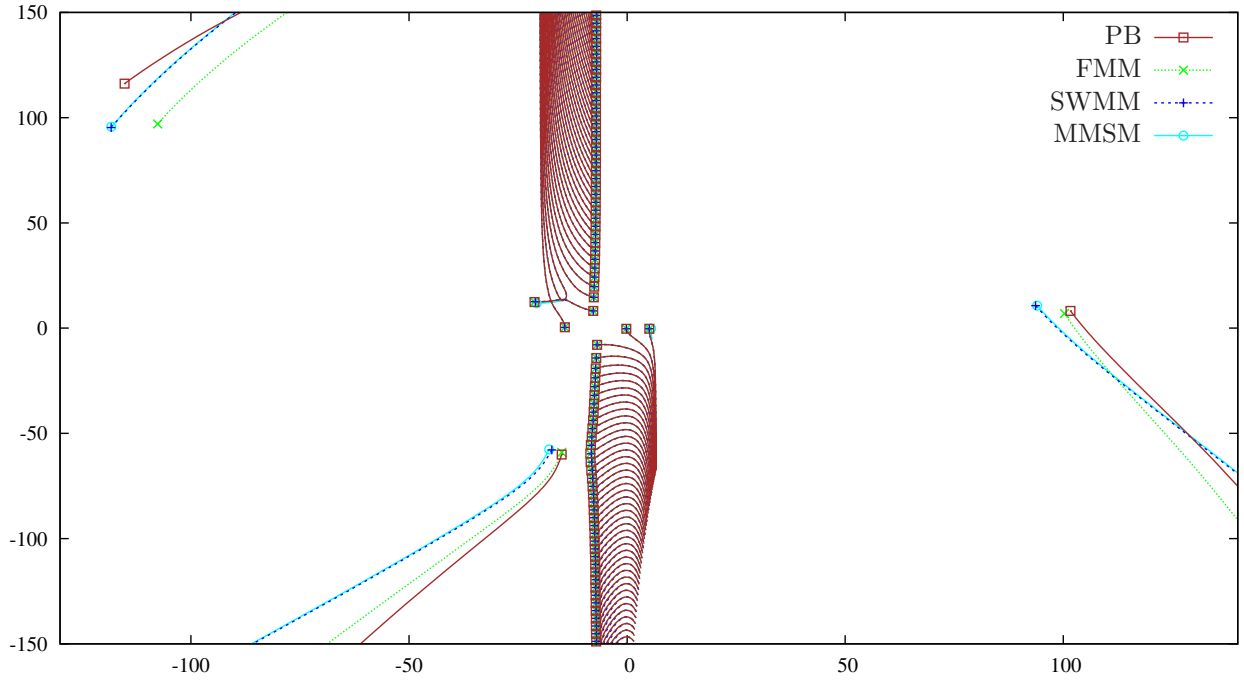

Figure 11: Briggs–Bers trajectories of modes in the complex k-plane for $\mathrm{Im}(\omega) \in [-100, 0]$ with $\mathrm{Re}(\omega) = 10$ for various dispersion relations. Parameters are as for figure 4: $m = 5$, a tanh boundary layer profile (15) with $\delta = 10^{-3}$ and $M = 0.5$, and a Helmholtz resonator impedance (29) with $\mathcal{R} = 1$, $d = 4/7$ and $L = 3.544024 \times 10^{-2}$. Dispersion relations: PB = Pridmore-Brown numerical modes, FMM = Full Modified Myers, SWMM = Short Wavelength Modified Myers, MMSM = Modified Myers Surface Mode.

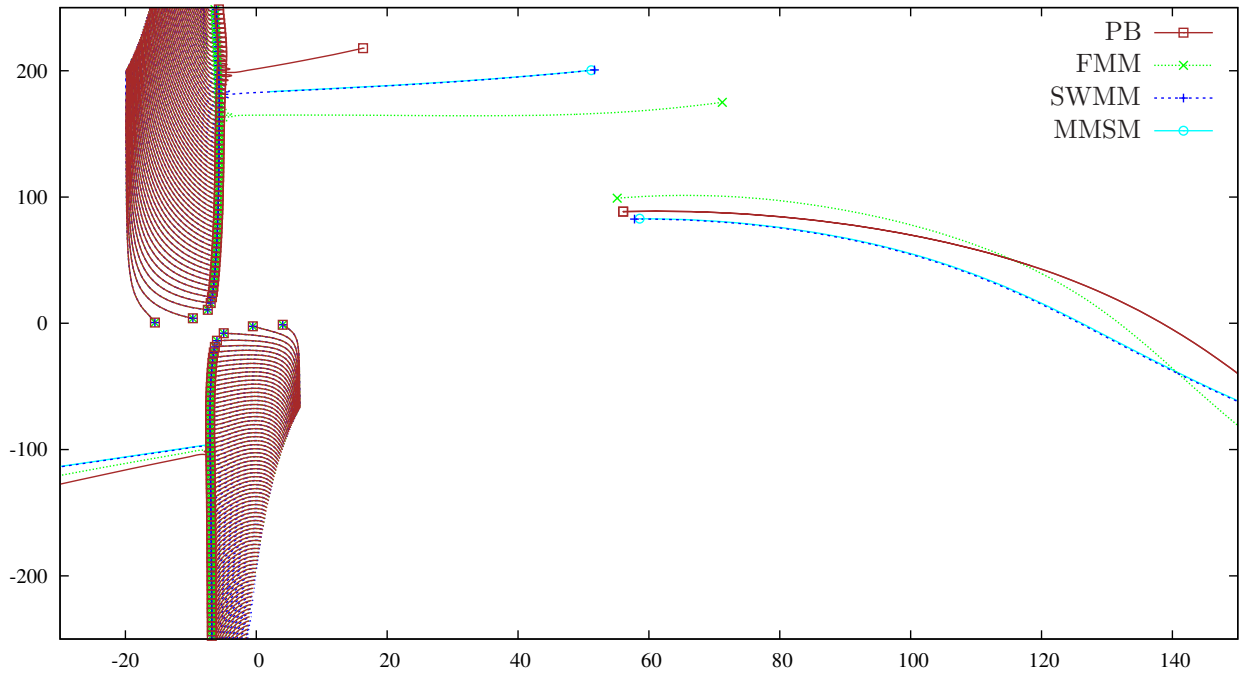

Figure 12: Briggs–Bers trajectories of modes in the complex k-plane for $\mathrm{Im}(\omega) \in [-100, 0]$ with $\mathrm{Re}(\omega) = 10$ for various dispersion relations. Parameters are as for figure 5a: $m = 5$, a tanh boundary layer profile (15) with $\delta = 10^{-3}$ and $M = 0.5$, and a Helmholtz resonator impedance (29) with $\mathcal{R} = 1$, $d = 4/7$ and $L = 0.11446$. Dispersion relations: PB = Pridmore-Brown numerical modes, FMM = Full Modified Myers, SWMM = Short Wavelength Modified Myers, MMSM = Modified Myers Surface Mode.

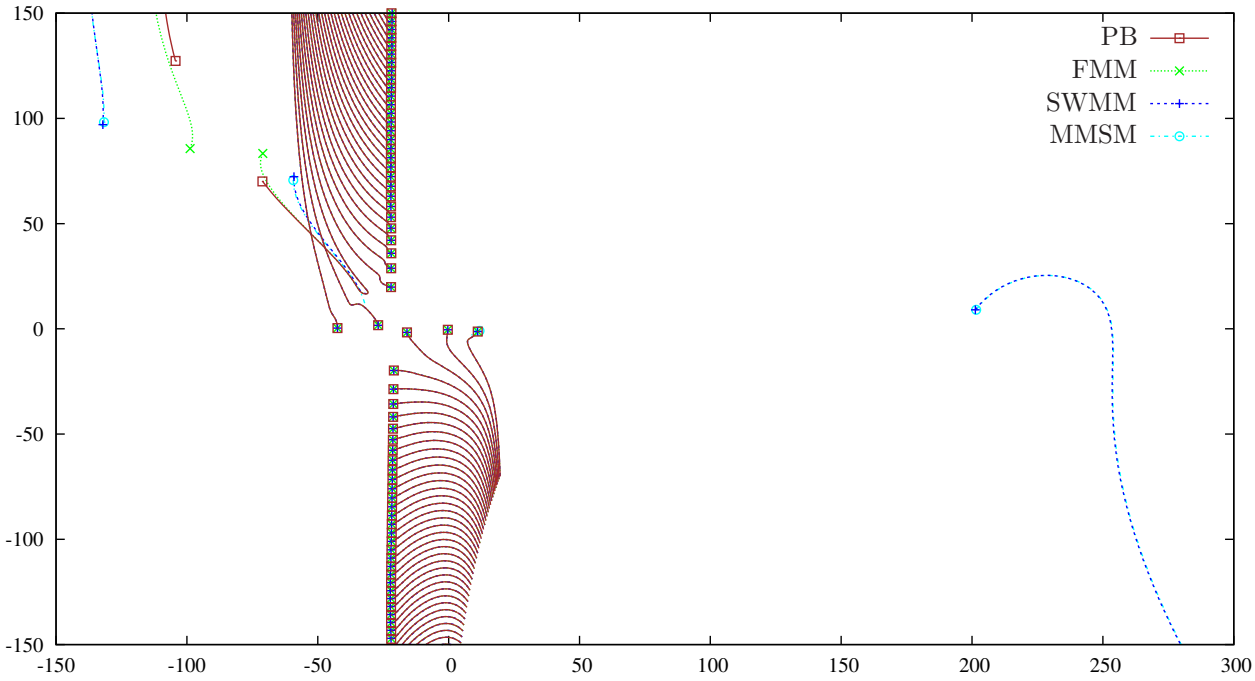

Figure 13: Briggs–Bers trajectories of modes in the complex k-plane for $\mathrm{Im}(\omega) \in [-100, 0]$ with $\mathrm{Re}(\omega) = 31$ for various dispersion relations. Parameters are as for figure 6*a*: $m = 24$, a tanh boundary layer profile (15) with $\delta = 10^{-3}$ and $M = 0.5$, and a Helmholtz resonator impedance (29) with $\mathcal{R} = 1$, $d = 4/7$ and $L = 0.109365$. Dispersion relations: PB = Pridmore-Brown numerical modes, FMM = Full Modified Myers, SWMM = Short Wavelength Modified Myers, MMSM = Modified Myers Surface Mode.

6 Conclusion

This paper considers the problem of determining the modes, and in particular the surface modes, of a cylindrical lined duct with coaxial flow and a thin sheared boundary layer. The surface mode approximation developed by Rienstra [6] and Brambley & Peake [7] is extended, with the thin boundary layer accounted for using a modified Myers boundary condition in the form proposed by Brambley [13]. The resulting dispersion relation is given in its most readily-useable form in (7), although a rescaled version of this reduces the number of free parameters by one. These free parameters are: the lining impedance Z; the centreline Mach number M; the acoustic spinning parameter $\lambda = \omega/\left(m\sqrt{1-M^2}\right)$; the boundary layer thickness measured on the length-scale of a far field wavelength $\tilde{h} = 2\omega\delta_1$; and the boundary layer shape parameters $\Delta_0 = \delta_0/(2\delta_1)$, $\Delta_k = \delta_k/(2\delta_1)$, and $\Delta_s = -M/\left(2R(1)U'(1)\delta_1\right)$. The first three parameters, Z, M and λ, are the same as for the uniform flow surface mode approximation [7]. Rather than the four surface modes supported by a uniform flow, a sheared boundary layer flow is shown to support up to six surface modes, as described for particular parameters in figures 2 and 3. This helps explain the patterns seen numerically by Vilenski & Rienstra [24] (for example, figure 8*b* of Ref. 24). For stability analysis, to leading order the only important measure of boundary layer thickness is δ_s, while to first order the boundary thickness scale δ_k also becomes important. While it is not possible to give here a complete catalogue of the behaviour of the surface modes in all possible parameter regimes (as was done in for the uniform case in Ref. 7) owing to the additional number of free parameters in the nonuniform case, the same analysis as presented here may be applied for other parameters without modification.

The fact that a sheared boundary layer flow supports a maximum of six surface modes, rather than the four supported by uniform flow, is important not only for finding all the modes for a given set of parameters, but also for ascertaining stability. Indeed, there are two modes in a region of the k-plane (labelled $\mathcal{R}_a$ in figure 2) that was predicted for uniform flow to contain only one, possibly unstable, surface mode. The stability analysis of section 5 suggests that one of these surface modes is indeed always a downstream-propagating convective instability while the other is a stable upstream-propagating evanescent wave, with the uniform flow surface mode usually not closely approximating either. Since these two modes will interchange places as the impedance varies around any collision point (as shown in figure 2), it is difficult to attach labels to these modes and say one is stable and the other unstable. Moreover, for sufficiently thin boundary layer thicknesses these two surface modes collide, as determined by (35), leading to an absolute instability that will dominate the behaviour of any convective instabilities.

The differential equation governing the pressure in a sheared flow is the Pridmore-Brown equation (1). Approximate solutions to this equation are found in this paper using a number of methods, being (in order of complexity and accuracy): directly numerically integrating the Pridmore-Brown equation (the PB results in figures); solving the modified Myers boundary condition of Brambley [13], derived asymptotically to include first order effects in the boundary layer thickness (the FMM results in figures); solving a short wavelength approximation to this modified Myers boundary condition (the SWMM results in figures); and assuming the flow to be constant and applying the Myers [2], or Ingard–Myers [3], boundary condition (the Myers results in figures). One result of this paper is therefore a comparison of these four methods for a number of different parameters, provided throughout §4. Unsurprisingly, the more complicated the method the more accurate the results, although the results here confirm the conclusions of Ref. 13 that the Myers boundary condition with uniform flow is a good approximation for the acoustic modes and a rather poor approximation for surface modes (although Gabard [14] also finds cases in which the uniform flow approximation is fairly inaccurate even for situations relevant to acoustic modes, while the modified Myers boundary condition of Ref. 13 remains accurate). The surface modes are predicted using a further surface-mode approximation [6] of the SWMM and Myers approximations (labelled MMSM and UMSM respectively in figures), with the MMSM and UMSM surface mode approximations being almost indistinguishable from the respective SWMM and Myers models they are approximating.

Section 4 gives a range of examples for particular parameters. While all of these examples have $M = U(0) = 0.5$ and $R(r) \equiv 1$, the analysis presented here is valid for general U and R. Two boundary layer profiles are used: the constant-then-linear profile (12) and the tanh profile (15), as used by Vilenski & Rienstra [24]. In general, these two boundary layer profiles are found to give similar results, in agreement with Gabard [14]. However, as shown in §4.2, it is possible to find parameters for which the linear profile supports an unstable surface wave while the tanh profile does not; moreover, this effect is shown to be due to the difference in boundary layer shape and not because one boundary layer is effectively thinner than the other.

While this paper has predominantly considered a mass–spring–damper or Helmholtz resonator impedance model, the numerical results can be expected to be indicative of general acoustic linings. For the majority of acoustic linings, the resistance $\mathrm{Re}(Z)$ remains nearly constant while the reactance $\mathrm{Im}(Z)$ varies significantly; for example, a Helmholtz resonator's reactance varies strongly with frequency and tuning parameters such as the depth of the resonator cell. The results of §4.3, therefore, demonstrate the range of surface mode behaviours for a general such acoustic lining, together with the accuracy of the predictions of this paper. The limit of a hard wall ($|Z| \to \infty$) is particularly interesting. For uniform flow, as $\mathrm{Im}(Z) \to -\infty$ four surface modes are present, with two surface modes tending to infinity in the k-plane, while as $\mathrm{Im}(Z) \to \infty$ no surface modes are present. This caused Rienstra (section 6 of Ref. 6) to propose a method for finding all modes by tracking modes from their hard-walled values as $\mathrm{Im}(Z)$ is reduced from $+\infty$. With a boundary layer present, we find that there are two surface modes tending to two finite values of k as $|Z| \to \infty$ in any direction (provided $\mathrm{Re}(Z) > 0$), with at least one of these values not corresponding to a hard-walled mode. It would seem, therefore, that for thin boundary layers this tracking procedure need not be restricted to reducing $\mathrm{Im}(Z)$ from $+\infty$ but does need to be augmented by finding at least one of the surface modes by independent means.

The examples of §4 show very good agreement between the full modified Myers solutions and the direct numerical solutions of the Pridmore-Brown equation, and generally very good agreement in the majority of cases between these and the short wavelength solution and the surface mode solution given by (7). While this good accuracy for the modified equations might be thought to be due to the very thin boundary layer used ($h = 10^{-3}$), in fact the small parameter of interest is the scaled boundary layer thickness $\tilde{h}$ given in (9), which for the examples given in the majority of §4 is $\tilde{h} \approx 0.04$, which is not very small. Moreover, section 4.4 shows qualitatively correct surface mode behaviour predicted by the modified equations even for $\tilde{h} = 0.5$, which is certainly not small. This suggests that the asymptotics that the modified equations are based on are relatively robust.

One aspect ignored by the current work is the presence of a critical layer and its associated branch cut in the complex k-plane. This branch cut is hinted at in figure 6 and shown explicitly in figure 8, since numerical solutions of the Pridmore-Brown equation and solutions of the full modified Myers dispersion relation are seen to "hide" behind this branch cut for certain values of the impedance Z. Investigation of the critical layer necessitates a different approach, as considered for linear boundary layer profiles in Ref. 16.

Acknowledgements

The support of a Junior Research Fellowship from Gonville & Caius College, Cambridge for the initial part of this research, and of a University Research Fellowship from the Royal Society for the latter part, are both

gratefully acknowledged. A preliminary version of this work [1] was presented as AIAA paper 2011–2736 at the 17th AIAA/CEAS Aeroacoustics Conference, 6–8 June 2011, Portland, Oregon, USA.

References

[1] E. J. Brambley. Surface modes in sheared flow using the modified Myers boundary condition. AIAA paper 2011-2736, 2011.
[2] M. K. Myers. On the acoustic boundary condition in the presence of flow. *J. Sound Vib.*, 71:429–434, 1980.
[3] U. Ingard. Influence of fluid motion past a plane boundary on sound reflection, absorption, and transmission. *J. Acoust. Soc. Am.*, 31:1035–1036, 1959.
[4] W. Eversman and R. J. Beckemeyer. Transmission of sound in ducts with thin shear layers — Convergence to the uniform flow case. *J. Acoust. Soc. Am.*, 52:216–220, 1972.
[5] B. J. Tester. The propagation and attenuation of sound in lined ducts containing uniform or "plug" flow. *J. Sound Vib.*, 28:151–203, 1973.
[6] S. W. Rienstra. A classification of duct modes based on surface waves. *Wave Motion*, 37:119–135, 2003.
[7] E. J. Brambley and N. Peake. Classification of aeroacoustically relevant surface modes in cylindrical lined ducts. *Wave Motion*, 43:301–310, 2006.
[8] E. J. Brambley. Fundamental problems with the model of uniform flow over acoustic linings. *J. Sound Vib.*, 322:1026–1037, 2009.
[9] S. W. Rienstra and M. Darau. Mean flow boundary layer effects of hydrodynamic instability of impedance wall. In *Proc. IUTAM Symposium on Computational Aero-Acoustics for Aircraft Noise Prediction, Southampton, 29–31 March*, 2010.
[10] S. W. Rienstra and M. Darau. Boundary-layer thickness effects of the hydrodynamic instability along an impedance wall. *J. Fluid Mech.*, 671:559–573, 2011.
[11] L. Joubert. *Asymptotic Approach for the Mathematical and Numerical Analysis of the Acoustic Propagation in a Strong Shear Flow*. PhD thesis, École Polytechnique, 2010. (in French).
[12] E. J. Brambley. A well-posed modified Myers boundary condition. AIAA paper 2010-3942, 2010.
[13] E. J. Brambley. A well-posed boundary condition for acoustic liners in straight ducts with flow. *AIAA J.*, 49(6):1272–1282, 2011. doi: 10.2514/1.J050723.
[14] G. Gabard. A comparison of impedance boundary conditions for flow acoustics. *J. Sound Vib.*, 332:714–724, 2013. doi: 10.1016/j.jsv.2012.10.014.
[15] E. J. Brambley and N. Peake. Stability and acoustic scattering in a cylindrical thin shell containing compressible mean flow. *J. Fluid Mech.*, 602:403–426, 2008.
[16] E. J. Brambley, M. Darau, and S. W. Rienstra. The critical layer in linear-shear boundary layers over acoustic linings. *J. Fluid Mech.*, 710:545–568, 2012. doi: 10.1017/jfm.2012.376.
[17] Y. Aurégan, R. Starobinski, and V. Pagneux. Influence of grazing flow and dissipation effects on the acoustic boundary conditions at a lined wall. *J. Acoust. Soc. Am.*, 109:59–64, 2001.
[18] Y. Renou and Y. Aurégan. On a modified myers boundary condition to match lined wall impedance deduced from several experimental methods in presence of a grazing flow. AIAA paper 2010-3945, 2010.
[19] Y. Renou and Y. Aurégan. Failure of the Ingard–Myers boundary condition for a lined duct: An experimental investigation. *J. Acoust. Soc. Am.*, 130:52–60, 2011. doi: 10.1121/1.3586789.
[20] Richard J. Briggs. *Electron-Stream Interaction with Plasmas*, chapter 2. MIT Press, 1964.
[21] Abraham Bers. Space–time evolution of plasma instabilities — absolute and convective. In A. A. Galeev and R. N. Sudan, editors, *Basic Plasma Physics*, volume 1 of *Handbook of Plasma Physics*, pages 451–517. North-Holland, 1983.
[22] D. C. Pridmore-Brown. Sound propagation in a fluid flowing through an attenuating duct. *J. Fluid Mech.*, 4:393–406, 1958.
[23] S. W. Rienstra and G. G. Vilenski. Spatial instability of boundary layer along impedance wall. AIAA paper 2008-2932, 2008.
[24] G. G. Vilenski and S. W. Rienstra. Numerical study of acoustic modes in ducted shear flow. *J. Sound Vib.*, 307:610–626, 2007.
[25] S. W. Rienstra. Impedance models in time domain, including the extended Helmholtz resonator model. AIAA paper 2006-2686, 2006.